A Vehicle Design and Optimization Model for On-Demand Aviation

Arthur Brown[1] and Wesley L. Harris[2]
Massachusetts Institute of Technology, Cambridge, MA, 02139

On-demand aviation refers to an envisaged air taxi service, using small, autonomous, vertical-takeoff-and-landing, battery-powered electric aircraft. A conceptual design and optimization tool for on-demand aviation is presented in this paper. The tool uses Geometric Programming, a class of optimization problems with extremely fast solve times and for which global optimality is guaranteed. The optimization model consists of a vehicle, a sizing mission, a revenue-generating mission, and a deadhead (non-passenger-carrying) mission. Cost per trip, including the additional cost due to the deadhead mission, is used as the objective function. Vehicle noise is computed during post-processing using a semi-empirical method. The tool is used to conduct a trade study between several different on-demand aircraft configurations. Four case studies are presented: one on a sizing plot useful for vehicle preliminary design; one on New York City airport transfers; one on technological assumptions in the near- and long-term; and one on low-noise design techniques. A series of sensitivity studies are also performed. Vehicle configurations with a higher lift-to-drag ratio, but a higher disk loading, generally weigh less and cost less to operate; configurations with a lower lift-to-drag ratio, but a lower disk loading, are quieter. An on-demand air service, even in the near term, is far superior in terms of cost per trip as compared to current helicopter air taxi operations. In the long term, costs become competitive with current car ridesharing services, indicating that on-demand aviation may one day become a widespread commute system for the masses. Technological assumptions and vehicle requirements, especially mission range, battery energy density, vehicle autonomy level, battery manufacturing cost, and reserve requirements, have significant impacts on vehicle weight and cost. Vehicle noise can be reduced through the careful selection of key design parameters. However, envisaged noise requirements cannot easily be met, even with the most generous long-term technological assumptions. Vehicle noise is therefore a critical issue for on-demand aviation; substantial engineering effort to reduce noise will be required.

Nomenclature

A	Rotor disk area
A_b	Rotor blade area
$A(f)$	A-weighting frequency response function
AR	Aircraft wing aspect ratio
ATC	Air Traffic Control
a	Speed of sound
B	Number of rotor blades
BVI	Blade-Vortex Interaction
C	Battery energy used
C_1	Vortex-noise interpolation constant 1

[1] Master's Candidate, Aerospace Computational Design Laboratory, MIT, 77 Massachusetts Avenue. Student member AIAA.
[2] Professor of Aeronautics and Astronautics, MIT, 77 Massachusetts Avenue. Fellow AIAA.

C_2	Vortex-noise interpolation constant 2
C_{D_0}	Aircraft 3D zero-lift drag coefficient
C_{d_0}	Rotor blade 2D zero-lift drag coefficient
C_L	Aircraft wing 3D lift coefficient
C_l	Rotor local blade lift coefficient, referenced to $V_{0.7}$
$\overline{C_l}$	Rotor mean lift coefficient
C_P	Rotor power coefficient
C_{P_i}	Rotor induced power coefficient
C_{P_p}	Rotor profile power coefficient
C_Q	Rotor torque coefficient
C_T	Rotor thrust coefficient
c	Average rotor blade chord
c_d	Cost of flying 1 deadhead mission
c_r	Cost of flying 1 revenue-generating mission
dB	Decibel
dBA	A-weighted decibel
DEP	Distributed Electric Propulsion
DNL	Day Night Average Sound Level
DOC	Direct Operating Cost
dr	Deadhead ratio
EASA	European Aviation Safety Administration
EPNL	Effective Perceived Noise Level (in dB)
e	Oswald efficiency
eVTOL	Electric VTOL
FAA	Federal Aeronautics Administration
FOM	Rotor figure of merit
f	Frequency
f_{peak}	Vortex-noise peak frequency
fr	Frequency ratio
GP	Geometric Program
h	Rotor blade projected thickness
IOC	Indirect Operating Cost
J_{mB}	Bessel function of the first kind, of order mB
K	Noise constant (6.1×10^{-11} $\frac{s^6}{ft^8}$)
K_2	Noise constant 2 (1.206×10^{-2} s^3/ft^3)
k	Aircraft induced power factor
k_i	Rotor induced power factor
$L_{A_{eq}}$	A-weighted Equivalent Continuous Sound Level
L_{AE}	A-weighted decibels, sound exposure level
L_{dn}	Day Night Average Sound Level
L/D	Vehicle lift-to-drag ratio
M_{tip}	Rotor tip Mach number
MMH/FH	Maintenance man-hours per flight hour
MTOW	Maximum Takeoff Weight
m	Harmonic number
N	Number of rotors
N_d	Number of deadhead missions
N_r	Number of revenue-generating missions
NPV	Net Present Value
ODA	On-Demand Aviation
ODM	On-Demand Mobility
PNL	Perceived Noise Level (in dB)
p	Effective sound pressure
p_0	Static air pressure
p_{m_L}	Root-mean-square loading pressure
p_{m_T}	Root-mean-square thickness pressure
p_{ref}	Reference sound pressure (2×10^{-5} Pa)
p_{total}	Total air pressure
$p(t)$	Acoustic pressure
Q	Rotor torque

R	Rotor radius
R_e	Effective rotor radius ($0.8R$)
RMS	Root Mean Square
r	Rotor blade radial location
SPL	Sound pressure level (in dB)
St	Strouhal number
s	Rotor solidity
T	Thrust generated by 1 rotor
T/A	Rotor disk loading
t	Rotor blade thickness
$t_{mission}$	Time to complete mission
t/c	Rotor blade thickness-to-chord ratio
V	Cruising flight speed
$V_{0.7}$	Rotor blade velocity at a radial location $r/R = 0.7$ (i.e. $0.7V_T$)
V_T	Rotor tip speed
V_{cruise}	Cruising flight speed
V_{loiter}	Loiter flight speed
VFR	Visual Flight Rules
VTOL	Vertical Takeoff and Landing
W	Vehicle weight
y	Observer ground location
z	Vehicle height above ground
α	Rotor blade angle of attack at a radial location $r/R = 0.7$
ΔS	Distance from noise source to observer
$(\Delta S)_{ref}$	Reference distance (500 ft)
η	System efficiency
θ	Observer azimuthal angle
ρ	Air density
Ω	Rotor angular velocity

I. Introduction

A. Background

On-Demand Aviation (ODA), also known as On-Demand Mobility (ODM) or eVTOL (Electric Vertical Takeoff and Landing), is an envisaged air taxi service. The service would use small, 1-4 place aircraft for trips of approximately 200 nautical miles or less [1]. Most proposed aircraft concepts are fully electric, although some are hybrid-electric. In general, multiple motors and propellers are used; this design strategy is known as Distributed Electric Propulsion, or DEP. DEP is enabled because electric motors, unlike internal-combustion engines, are efficient at a wide range of sizes. The aircraft are capable of VTOL (Vertical Takeoff and Landing). On-demand aviation offers a number of advantages over existing transport solutions, including:

- Greatly reduced commute times and/or greatly increased Mobility Reach (accessible land area with a given commute time [1]), by avoiding gridlock
- Lower energy costs, due to the use of electricity instead of gasoline
- Reduced environmental impact (in terms of noise, climate change, lead, and other emissions), also due to the use of electric propulsion
- Lower (or no) pilot operating costs, due to autonomy

Uber published a white paper in October 2016 outlining their vision for an on-demand aviation service, which they call Uber Elevate [2]. In it, they describe what they see at the key market feasibility barriers, including battery technology, vehicle efficiency, air traffic control, cost, safety, noise, and emissions. Uber also held a summit in Dallas in April 2017 to bring together stakeholders from industry, academia, and government [3].

An image of Uber's vision is shown in Figure 1.

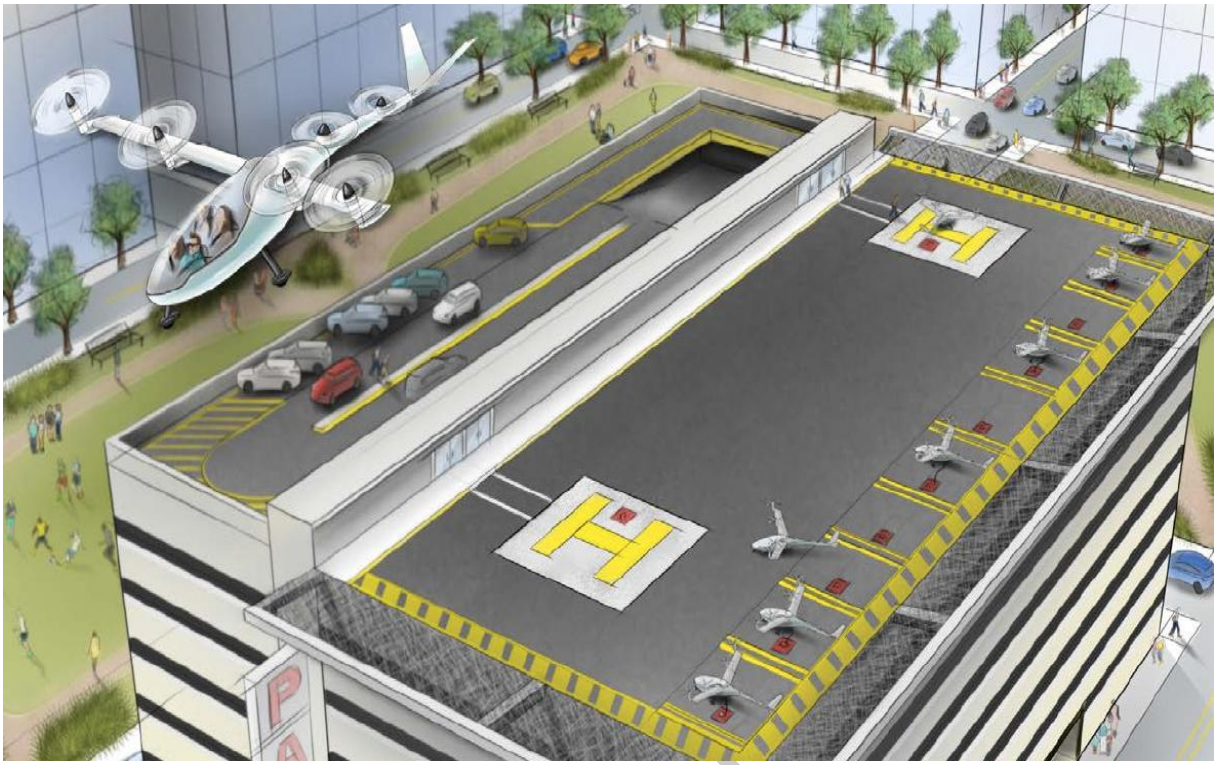

Fig. 1 The envisaged Uber Elevate service [2].

B. Research Goals

The goal of this research is to conduct a trade study between various proposed vehicle configurations. Dozens of companies are working on eVTOL aircraft designs, including Joby Aviation, Terrafugia, Lilium Aviation, A^3 by Airbus, and Aurora Flight Sciences. A variety of fundamentally different design approaches are employed. For example, Joby Aviation's S4 and Terrafugia's TF-X are both tilt-rotor designs; Lilium Aviation uses a tilt-duct design; and Airbus' Vahana concept is a tilt-wing design. In addition, Aurora Flight Sciences presented a lift + cruise design (i.e. a design with separate rotors for cruise and for hover, with no folding or tilting components) at the Uber Elevate summit [3]. Other postulated configurations include the multirotor, the autogyro, the conventional helicopter, the tilt duct, the coaxial-rotor helicopter, and the compound helicopter [4]. This research aims to provide guidance to vehicle designers on the strengths and weaknesses of each configuration, with a particular focus on vehicle noise. A series of sensitivity studies are also conducted, to evaluate the influence of key design parameters and vehicle requirements on the results.

II. Methodology

An optimization tool was developed to conduct a top-level trade study between the various configurations, as well as to determine sensitivities. The tool is formulated as a geometric program (GP), a type of constrained optimization problem. Geometric programs require that the objective function and constraints be posed in a special form. In return, they offer extremely fast solve times, require no initial guesses, and guarantee a globally optimal solution. See Reference [5] for a discussion of geometric programming, and Reference [6] for an example of its application to aircraft design.

The tool uses vehicle and mission models similar to those used by McDonald & German [4]. Some key vehicle parameters, such as empty weight fraction and battery energy density, are held constant between

vehicle configurations. Other parameters, such as cruising speed, cruise lift-to-drag ratio, and hover disk loading, are varied between configurations, using representative values for a given configuration.

However, in this study, optimization is used instead of sizing. Instead of assuming a fixed vehicle weight and empty weight fraction, then computing the range, this work assumes a fixed empty weight fraction and mission range, then computes the required vehicle weight during the optimization process. This means that all configurations have the same range, enabling comparisons between them.

A. Vehicle Model

1. Components

The vehicle model is divided into five components: structure, battery, electrical system, avionics, and rotors. The structural model assumes an empty weight fraction, relative to the maximum takeoff weight; the battery model assumes a battery specific energy and specific power, and sizes the battery accordingly. 20% of the battery energy is unusable (even for reserves), to prevent current spikes at low charge levels and also to extend battery life. This is in accordance with the practice of Reference [4].

The electrical system applies a constant efficiency to the power coming from the batteries in both hover and cruise; the avionics model is only used for cost modeling if vehicle autonomy is enabled (discussed in Section II D); and the rotor model is only used in hover. The structure and battery have their own weight models; the weight of the other three components are bookkept under empty weight.

2. Cruise Performance

The range and endurance of an electric aircraft in cruise can be computed using Equations 1 and 2 respectively:

$$Range = \eta \frac{L}{D} \frac{C}{W} \tag{1}$$

$$Endurance = \eta \frac{L}{D} \frac{C}{VW} \tag{2}$$

$\frac{L}{D}$ is the vehicle lift-to-drag ratio in cruise, C is the battery energy used, W is the vehicle weight, and V is the cruising speed. η is the system efficiency, equal to the product of electric and propulsive efficiency. Electrical efficiency accounts for losses due to the wires, controller, and motors; a value of 90% is used in both cruise and hover. For a propeller-driven aircraft, propulsive efficiency is equal to propeller efficiency; a value of 85% is used.

3. Hover Performance

In hover, the rotors must produce thrust equal to vehicle weight; the power required to generate this thrust must be computed. The rotor model developed for this purpose uses an extension of actuator-disk theory, using equations from Chapter 3 of Reference [7]. The effects of non-uniform downwash and blade profile drag are included.

The rotor thrust coefficient is defined in Equation 3:

$$C_T = \frac{T}{\frac{1}{2}\rho {V_T}^2 A} \tag{3}$$

C_T is the rotor thrust coefficient, T is the thrust generated by the rotor, ρ is the air density, V_T is the rotor tip speed, and A is the rotor disk area (πR^2, where R is the rotor radius).

The power coefficient is defined in Equation 4:

$$C_P = \frac{P}{\frac{1}{2}\rho {V_T}^3 A} \tag{4}$$

C_P is the power coefficient, while P is the power required to turn the rotor. C_P is related to the ideal and profile power coefficients through Equations 5, 6, and 7:

$$C_P = k_i C_{P_i} + C_{P_p} \tag{5}$$

$$C_{P_i} = \frac{1}{2} {C_T}^{3/2} \tag{6}$$

$$C_{P_p} = \frac{1}{4} s C_{d_0} \tag{7}$$

C_{P_i} is the ideal power coefficient. If profile drag is neglected and the blade lift distribution is elliptical, then C_{P_i} is equal to C_P. The induced power factor k_i accounts for non-uniform lift distribution, while the profile drag coefficient C_{P_p} accounts for profile drag. s is the rotor solidity, computed using Equation 8:

$$s = \frac{A_b}{A} = \frac{BcR}{\pi R^2} \tag{8}$$

A_b is the rotor blade area, equal to the product of the number of blades B, average blade chord c, and blade radius R.

Figure of merit FOM is defined as the ratio of ideal to actual power required in hover. It can be computed using Equation 9:

$$FOM = \frac{C_{P_i}}{C_P} \tag{9}$$

While not required by the optimization model, torque is required for the purpose of computing noise during post-processing. Equation 10 relates torque Q and torque coefficient C_Q:

$$C_Q = \frac{Q}{\frac{1}{2}\rho {V_T}^2 AR} \tag{10}$$

Torque and power coefficients are equal.

Finally, "[the rotor] mean lift [coefficient] is that which, applied uniformly across the blade span, would give the same thrust as the total blade" [7]. Rotor mean lift coefficient, denoted as $\overline{C_l}$, can be calculated using Equation 11:

$$\overline{C_l} = \frac{3C_T}{s} \tag{11}$$

Rotor tip speed is a design variable. The upper limit on tip speed is a limit on the tip Mach number, while a lower limit is set by limiting the blade mean lift coefficient.

Calculations are performed on a per-rotor basis. Standard sea-level values for ρ (air density) and a (speed of sound) are used.

The rotor aerodynamic model was validated using experimental data from Bagai & Leishman [8], as given by Leishman [9]. The data was obtained using a series of experiments conducted on a four-bladed model helicopter rotor, with a radius of 32.5 inches and a solidity of 0.098. Results are shown in Figure 2.

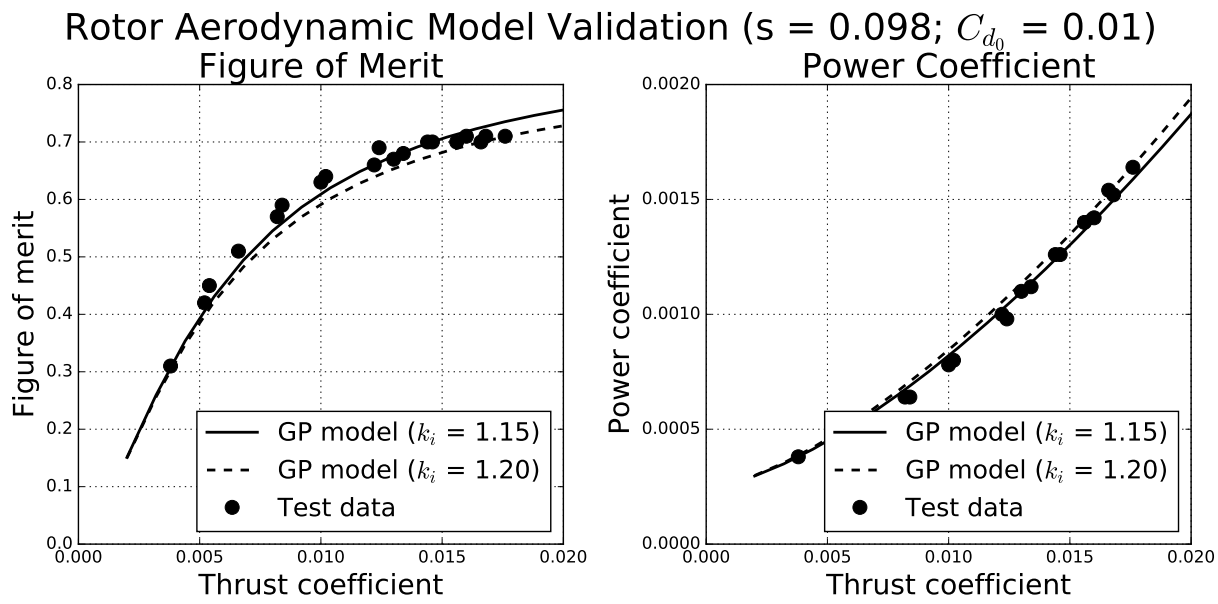

Fig. 2 Validation of the rotor aerodynamic model.

Values of k_i and C_{d_0} of 1.15 and 0.01 respectively are recommended by Leishman. Figure 2 shows that using this set of parameters results in a reasonable approximation of the experimental data. However, most of the optimized designs in this study have thrust coefficients in the range of 0.025-0.035, higher than the data in Figure 2. On-demand air vehicles are capable of higher thrust coefficients relative to helicopters. This is due to the higher limits on blade mean lift coefficient (discussed in Section III A), directly leading to higher thrust coefficients through Equation 11. A value of $k_i = 1.2$ was used to better match the available data at higher thrust coefficients.

Parameters used by the rotor model are given in Table 2.

Table 2 Rotor model parameters.

Parameter	Symbol	Value
Induced power factor	k_i	1.2
Blade zero-lift drag coefficient	C_{d_0}	0.01
Rotor solidity	s	0.1
Tip Mach number (upper limit)	M_{tip}	0.9

B. Noise Model

A model for vehicle noise is developed in this section. The model is not compatible with geometric programming, so it was not integrated into the optimization model. Instead, vehicle noise is computed during post-processing.

1. Importance of Noise

Low noise is essential in order to achieve community acceptance for on-demand aviation. Community opposition to increased noise is already an important consideration for commercial airliners [10], supersonic jet concepts [11], and helicopters [12]. Both the Federal Aeronautics Administration (FAA) and European Aviation Safety Administration (EASA) already have noise limits in place for various types of aircraft, but Uber anticipates that a much stricter standard will be required for on-demand aviation.

A significant portion of the Uber Elevate paper is devoted to defining a set of quantitative noise goals. They eventually select a target noise level of 62 dBA (A-weighted decibels) with the vehicle hovering 500 ft

overhead. This is half the noise generated by a medium-size truck at 50 ft, and comparable to a Prius at 25 ft [2]. A-weighting is discussed further in Section II B 7.

2. Noise Metrics

Metrics for aircraft noise measurement can be divided into five categories and/or steps, with each category building upon the previous one. The first and simplest category is unweighted sound pressure level, or SPL. SPL is defined in Appendix A; it is measured in decibels (dB).

Humans are capable of hearing sounds at frequencies between about 20 Hz and 20 kHz; also, human ears have different responses at different frequencies [13]. For example, humans will perceive a 2.5-kHz tone as being much louder than a 40-Hz tone if the two tones have identical sound pressure levels. The second step is therefore to introduce noise exposure levels, noise metrics that takes human response into account [14]. Examples include A-weighted decibels (dBA) and perceived noise level (PNL). dBA is designed such that the average human will perceive two sounds with the same noise exposure level as being equally loud, regardless of frequency. Meanwhile, PNL is based upon annoyance criteria rather than equal loudness.

The third step is to introduce effective noise levels. Metrics in this category adjust the noise exposure level to account for the length of time of the noise event. [14]. Examples include Single Event Level (SEL), which when applied to A-weighted decibel measurements is typically referred to as L_{AE}. "[L_{AE}] is the [equivalent] A-weighted sound pressure level lasting one second that contains the same energy as an entire aircraft event such as takeoff or overflight" [2]. Meanwhile, Effective Perceived Noise Level (EPNL) is based upon PNL, and is the standard metric for aircraft noise regulations [14].

The fourth step is to introduce noise indices, which adjust the effective noise level to account for the number of noise sources present. Variation of noise levels with time is also accounted for. Examples include the A-weighted Equivalent Continuous Sound Level ($L_{A_{eq}}$) and the Day Night Average Sound Level (L_{dn} or DNL).

The final step is to introduce noise criteria. A simple example is the percentage of the population in a given area that experiences noise above a certain level [14].

This work is concerned with metrics in the first and second category; all noise data uses either unweighted or A-weighted decibels. However, two additional noise metrics (in addition to A-weighted sound pressure level) are defined in the Uber white paper: long-term annoyance (measured in terms of the DNL) and short-term annoyance (measured in terms of the SEL). Future work should focus on incorporating these metrics, as well as metrics in the other categories listed above.

3. Sources of Noise

Lowson and Ollerhead conducted a comprehensive review of the helicopter noise prediction problem. [15]. A list of helicopter noise sources, in decreasing order of importance, is included in that reference:

- Blade slap (when it occurs)
- Piston-engine exhaust noise
- Tail-rotor rotational noise
- Main-rotor vortex noise
- Main-rotor rotational noise
- Gearbox noise
- Turbine engine noise

The noise problem for an on-demand aircraft is more straightforward than that of a helicopter, because gearbox noise and turbine engine noise are absent. Piston-engine exhaust noise is also absent, unless the vehicle is a hybrid. Therefore, the noise model in this report accounts for blade slap, rotational noise, and vortex noise.

4. Blade Slap

Blade slap is the most significant source of noise for a helicopter. Three causes of blade slap are identified in Reference [16]. The first is shockwave formation, which typically occurs at high rotor blade tip Mach numbers. It is shown in Section III B that optimized tip Mach numbers for on-demand electric aircraft are typically in the range of 0.35-0.55, significantly lower than values typical for helicopters [7]. Therefore, this form of blade slap is neglected. Blade stall is also cited as a cause of blade slap, but this problem can be mitigated by the selection of appropriate constraints on blade mean lift coefficient. In addition, blade stall tends to be a problem in cruise, rather than in hover. Therefore, concepts that use wings instead of rotors in cruise should not suffer from blade stall.

The final form of blade slap is known as blade-vortex interaction (BVI); it occurs when one rotor blade passes through the bound vortex emanating from another blade. This form of blade slap is common during descent to landing. Helicopters can avoid this form of noise using correct approach and departure procedures, examples of which are given in Reference [17]. It is hypothesized in this work that on-demand electric aircraft can take advantage of similar procedures. Therefore, BVI noise is neglected as well.

5. Rotational Noise

Rotor noise in the absence of blade slap can be divided into two main components: rotational noise, which occurs at integer multiples of the blade passage frequency (blade rotational frequency $\times$ number of rotor blades); and vortex noise, which is broadband in nature. Rotational noise is also referred to as harmonic noise.

Rotational noise can be divided into two categories: loading noise, which is a direct consequence of thrust generation; and thickness noise, caused by finite rotor blade thickness. These two forms of noise can be modeled by the Gutin and Deming formulae respectively. They are derived in equivalent-radius form in Appendix C. The resulting noise model is repeated here as Equations 12, 13, and 14:

$$p_{m_L} = \frac{mB\Omega}{2\sqrt{2}\pi a(\Delta S)}\left[T\cos\theta - Q\frac{a}{\Omega R_e^2}\right]J_{mB}\left(\frac{mB\Omega}{a}R_e\sin\theta\right) \tag{12}$$

$$p_{m_T} = \frac{-\rho(mB\Omega)^2 B}{3\sqrt{2}\pi(\Delta S)}ctR_e J_{mB}\left(\frac{mB\Omega}{a}R_e\sin\theta\right) \tag{13}$$

$$SPL = 10\log_{10}\left[N\left(\frac{p_{m_L}^2 + p_{m_T}^2}{p_{ref}^2}\right)\right] \tag{14}$$

p_{m_L} and p_{m_T} are the root mean square (RMS) sound pressures for loading and thickness noise respectively. m is the harmonic number (a positive integer), N is the number of rotors, B is the number of rotor blades, Ω is the rotor angular velocity, a is the speed of sound, and ΔS is the distance between the rotor and the observer. T is the rotor thrust, Q is the rotor torque, and θ is the observer azimuthal location. ρ is the air density, c is the blade chord, and t is the blade maximum thickness. J_{mB} is a Bessel function of the first kind of order mB. A diagram showing ΔS and θ is given in Figure 3.

An effective rotor radius of $R_e = 0.8R$ is recommended by Reference [18], and is used throughout this work. Blade chord is estimated using the definition of solidity (Equation 8). Since the NACA 0012 airfoil is a traditional choice for helicopter rotor blades [7], the blade thickness is calculated using an assumed thickness-to-chord ratio of 12%. Finally, p_{ref} is the reference pressure, equal to 2×10^{-5} Pa.

Unless otherwise stated, all rotational noise calculations assume a five-bladed rotor. Combined with the solidity value from Table 2, this results in a blade aspect ratio of 15.9, a reasonable compromise between blade efficiency and structural integrity for helicopters [7].

Note that $\theta = 180°$ directly underneath an on-demand aircraft, so $J_{mB}\left(\frac{mB\Omega}{a}R_e\sin\theta\right) = 0$. Therefore, rotational noise is negligible for an observer underneath the aircraft, something that is not true for vortex noise. Because the Uber noise requirement is for an observer 500 ft underneath the aircraft, all studies (unless otherwise noted) neglect rotational noise. This assumption is investigated further in Section III B 2.

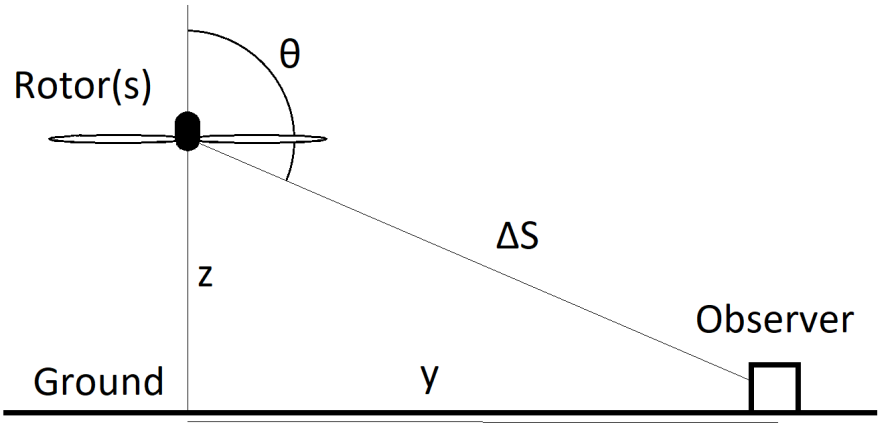

Fig. 3 Azimuthal angle diagram.

6. Vortex Noise

A model for vortex noise is derived in Appendix D A, and is repeated here as Equation 15:

$$SPL = 20\log_{10}\left[K_2 \frac{V_T}{\rho(\Delta S)}\sqrt{\frac{NT}{s}\left(\frac{T}{A}\right)}\right] \tag{15}$$

T/A is the rotor disk loading; K_2 is a constant, equal to $1.206 \times 10^{-2}\ s^3/ft^3$.

All of the non-constant parameters in Equation 15 both provide a benefit to vehicle sizing and reduce noise. For example, K_2, ρ, and ΔS are constants. Meanwhile, lowering tip speed, increasing rotor solidity, and decreasing rotor disk loading all result in sizing benefits. Finally the product of number of rotors and rotor thrust is equal to vehicle weight; a lighter vehicle both costs less (see Section II D) and is quieter.

Equation 15 was validated using data in Reference [19] for two different helicopter main rotors: the CH-3C and the CH-53A. Results are given in Appendix D A. It is shown that the model is accurate to within 3 dB of test data.

Although vortex noise is broadband in nature, it has a peak frequency (frequency at which the amplitude is highest). It can be estimated using Equation 16 [16]:

$$f_{peak} = \frac{(V_{0.7})St}{h} \tag{16}$$

f_{peak} is the vortex-noise peak frequency (in Hz), St is the Strouhal number, $V_{0.7}$ is the blade velocity at a radial location $r/R = 0.7$ (i.e. 0.7 times the tip speed), and h is the projected blade thickness (see Appendix D B). An estimate of $St = 0.28$ is used; this is a reasonable value for a helicopter [16].

Once peak frequency is known, the vortex-noise frequency spectrum can be obtained using the method in Appendix D B. This is required if noise weighting schemes are to be applied.

7. A-Weighting Scheme

As discussed in Section II B 2, human ears have different responses at different frequencies. Various decibel weighting schemes have been proposed to account for this, the most widely used of which is the A-weighting scheme. This scheme applies a response function to a given sound pressure level, in order to compensate for the frequency response of the human ear. The A-weighting response function $A(f)$ as a function of frequency is plotted in Figure 4.

Figure 4 reveals that $A(f)$ is maximized at a frequency of approximately 3 kHz, indicating that humans are particularly sensitive to sounds at this frequency. In order to reduce subjective annoyance, the designer should strive to avoid sound frequencies near 3 kHz as much as possible.

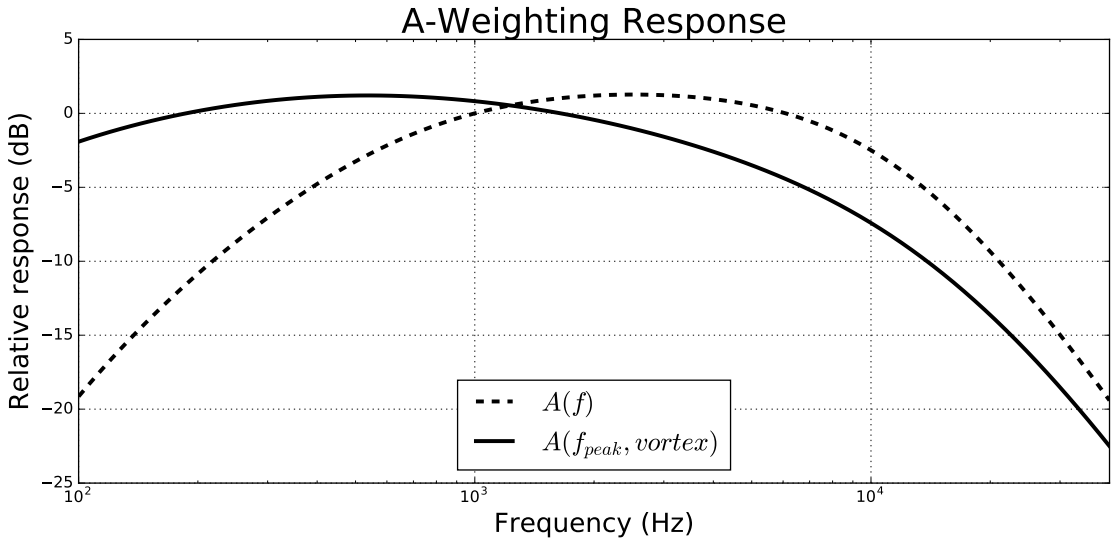

Fig. 4 The A-weighting response function.

The Gutin and Deming model for rotational noise produces a discrete array of frequencies and sound pressure levels. Therefore, the A-weighted sound pressure level can be obtained by applying $A(f)$ to the sound pressure level for each harmonic, then adding the results using the method in Appendix B. This method cannot be applied to vortex noise because the resulting frequency spectrum is continuous. Instead, an approximate procedure for applying A-weighting to vortex noise is derived in Appendix D C.

It is shown in Appendix D B that the vortex-noise frequency spectrum ranges from $0.5f_{peak}$ to $16f_{peak}$. Therefore, most of the sound produced is at frequencies higher than the peak frequency; the peak frequency at which human ears are most sensitive is therefore somewhat lower than 3 kHz. Figure 4 also shows $A(f)$ as a function of f_{peak}, revealing a maximum around $f_{peak} = 600$ Hz. The designer should therefore strive to obtain a peak frequency as far away from 600 Hz as possible.

A-weighted sound pressure level is known to be far from perfect in predicting human perception of loudness, in part because of its bias against low frequencies [13]. It is used in this study for two primary reasons. First of all, it is by far the most common metric for noise prediction, allowing comparisons with data from other noise sources such as cars and helicopters (see Section II B 1). Secondly, it is often used for regulatory purposes. Therefore, it forms a reasonable starting point, and is used throughout this study.

8. Limitations

The noise model is not immediately applicable to all vehicle configurations. For example, a coaxial helicopter will produce additional noise due to the interaction of the flow field between the rotors. This effect was not taken into account.

Conventional and compound helicopters have tail rotors, to counteract the torque of the main rotor. According to Lowson and Ollerhead, helicopter tail rotors are subjectively louder than main rotors [15]. Many modern helicopters use shrouded tail rotors, which substantially reduce noise [20]. Therefore, it is assumed that the conventional and compound helicopters use shrouds, and tail-rotor noise is neglected. This approximation should be treated with extreme caution.

C. Mission Model

The mission model is also similar to that in Reference [4], with three different mission profiles:

- A sizing mission, which the aircraft must be capable of flying.
- A revenue mission, in which the aircraft is carrying paying passengers.

- A deadhead mission, in which the aircraft is merely being repositioned for its next revenue-generating flight and no passengers are carried.

The sizing mission includes a longer hover time relative to the revenue and deadhead missions; it also includes a reserve. Three reserve options are available. The first is a 20-minute loiter time, required by the FAA for helicopter VFR (Visual Flight Rules) operations [21]. This requirement applies both during the day and at night, and would be applicable if on-demand vehicles are certified as helicopters. The second reserve option is a 30-minute loiter time, required for the FAA for aircraft VFR (Visual Flight Rules) operations during the day [20]. This requirement would be applicable if on-demand vehicles are certified as aircraft. The final option is a 2-nmi diversion distance, included in case a special regulatory class is created for eVTOL aircraft. A similar option was used by Reference [4]; this option is hereafter referred to as the Uber reserve requirement.

Two crew options are available: piloted and autonomous. If the mission is piloted, the pilot is assumed to add 190 lbs to the vehicle weight. If the mission is autonomous, no weight penalty is applied. 200 lbs per passenger is assumed.

Mission-profile descriptions are given in Table 3.

Table 3 Mission profiles.

Segment	Sizing (FAA aircraft)	Sizing (FAA helicopter)	Sizing (Uber reserve)	Revenue and Deadhead
1	120s hover	120s hover	120s hover	30s hover
2	Cruise	Cruise	Cruise	Cruise
3	30-minute loiter	20-minute loiter	2-nmi diversion	30s hover
4	120s hover	120s hover	120s hover	Time on ground

Segment 4 of the revenue-generating and deadhead missions (i.e. time on ground) includes a segment time constrained by one of two factors. Firstly, the time has to be greater than 5 minutes, to allow for passenger loading/unloading, safety checks, etc. Secondly, the vehicle is assumed to be charging at the same time; all of the energy used during the mission is replenished. A 200 kW charger is assumed for the purposes of computing charging time.

Cruising speed and cruise lift-to-drag ratio were provided as input parameters for each configuration. These numbers are used in cruise, and also for the reserve segment if the Uber reserve requirement is used. However, the FAA reserve requirement is a loiter requirement, as opposed to a cruise requirement. For this reason, the optimal lift-to-drag ratio and flight speed differ from the cruise values.

If a parabolic drag polar is assumed, Equations 1 and 2 can be written as Equations 17 and 18 respectively:

$$Range = \eta \frac{C_L}{C_{D_0} + kC_L^2} \frac{C}{W} \tag{17}$$

$$Endurance = \eta \left[\frac{\rho S C_L}{2W}\right]^{1/2} \frac{C_L}{C_{D_0} + kC_L^2} \frac{C}{W} \tag{18}$$

C_L is the wing three-dimensional lift coefficient, C_{D_0} is the aircraft three-dimensional zero-lift drag coefficient, and k is the aircraft induced power factor. All values are referenced to the wing area S. k is equal to $\frac{1}{\pi e AR}$, where e is the Oswald efficiency and AR is the wing aspect ratio.

The conditions for maximum range and endurance can be obtained by differentiating Equations 17 and 18 respectively, with respect to lift coefficient. This yields the values for lift coefficient, airspeed, and lift-to-drag ratio in Table 4.

Table 4 Flight conditions for maximum range and endurance.

	Lift coefficient	Airspeed	Lift-to-drag ratio
Max range	$C_L = \left[\frac{C_{D_0}}{k}\right]^{1/2}$	$V = \left[\frac{2W}{\rho S}\right]^{1/2} \left[\frac{k}{C_{D_0}}\right]^{1/4}$	$\frac{L}{D} = \frac{1}{2}\left[\frac{1}{kC_{D_0}}\right]^{1/2}$
Max endurance	$C_L = \left[\frac{3C_{D_0}}{k}\right]^{1/2}$	$V = \left[\frac{2W}{\rho S}\right]^{1/2} \left[\frac{k}{3C_{D_0}}\right]^{1/4}$	$\frac{L}{D} = \frac{1}{4}\left[\frac{3}{kC_{D_0}}\right]^{1/2}$

Therefore, if the cruising speed and lift-to-drag ratio for a given configuration are known, the loiter speed and lift-to-drag ratio can be estimated using Equations 19 and 20 respectively:

$$V_{loiter} = \left[\frac{1}{3}\right]^{1/4} V_{cruise} \tag{19}$$

$$\left(\frac{L}{D}\right)_{loiter} = \frac{\sqrt{3}}{2}\left(\frac{L}{D}\right)_{cruise} \tag{20}$$

The net effect of Equations 19 and 20 is to reduce power consumption (and by extension, energy use) during the loiter segment. This in turn provides a benefit to battery sizing. These adjustments were implemented in the optimization tool.

D. Cost Model

The cost model uses both the revenue mission and the deadhead mission. Costs are divided into two categories: capital expenses, and operating expenses. Key input parameters for the cost model are given in Table 5.

Table 5 Parameters used by the cost model.

Parameter	Value
Vehicle cost per unit empty weight	\$350 per lb
Avionics cost per aircraft (assuming vehicle autonomy is enabled)	\$60,000
Battery cost per unit energy capacity	\$400 per kWh
Pilot wrap rate	\$70 per hour
Pilots per aircraft (assuming a piloted mission)	1.5
Aircraft per bunker pilot (assuming an autonomous mission)	8
Mechanic wrap rate	\$60 per hour
Price of electricity	\$0.12 per kWh
Maintenance man-hours per flight hour	0.6
Deadhead ratio	0.2

1. Capital Expenses

Capital expenses are subdivided into three categories: vehicle purchase price, battery purchase price, and avionics purchase price. Vehicle purchase price is computed using a fixed price per unit empty vehicle weight, while battery purchase price is computed using a fixed price per unit energy capacity. If vehicle autonomy is enabled, the avionics add a fixed amount per aircraft. Avionics cost is neglected if vehicle autonomy is not enabled. These last two assumptions are identical to those in Reference [2].

First-order estimates for vehicle cost per unit empty weight were obtained for several different vehicle categories, ranging from business jets to electric cars. A summary of the results is in Table 6.

Table 6 Weight and cost estimates for several representative vehicles. Battery weight and cost were deducted from the Model S estimates by assuming a vehicle curb weight, purchase price, battery weight, battery energy density, and battery cost of 4,749 lbf, $70,000, 1,200 lbf, 200 Wh/kg, and $200 per kWh respectively.

Vehicle	Vehicle type	Empty weight (lbf)	Price ($US)	Price per unit empty weight
Cessna Citation Mustang	Very light jet	5,600	$3,350,000	$598.2
Robinson R44	Light helicopter	1,450	$425,000	$293.1
Cessna 172R	General-aviation aircraft	1,691	$274,900	$162.6
Ferrari 488	Sports car	3,362	$272,700	$81.1
Tesla Model S (75D)	Electric car	3,549	$48,182	$13.6
Honda Accord	Sedan	3,170	$22,455	$7.1

Table 6 shows that cost per unit empty weight varies widely depending on the vehicle type. Therefore, a relatively conservative estimate of $350 per lb is used. However, if production rates increase to levels approaching those typical in the automotive industry, Table 6 shows that significant cost savings are expected. Meanwhile, battery prices per unit energy capacity are based upon Department of Energy projections, as referenced in [2].

Capital expenses are then amortized over the mission, in order to estimate their effects on the cost of providing air taxi service. In financial terms, this is analogous to straight-line depreciation with zero salvage value. Vehicle and avionics costs are amortized using a 20,000-hour vehicle life, while the battery is amortized using a 2,000-cycle battery life.

2. Operating Expenses

Operating expenses are divided into direct operating cost (DOC) and indirect operating cost (IOC). Direct operating cost is further divided into three categories: pilot cost, maintenance cost, and energy (electricity) cost.

Pilot and maintenance costs are estimated using wrap rates, which include salary payments as well as benefits, overhead, training, administrative costs, etc [20]. Wrap rates of $50-150 per hour for pilots and $53-67 per hour for mechanics are typical [22].

Pilot and maintenance cost per mission are then computed using Equations 21 and 22 respectively:

$$Pilot\ cost = (Pilot\ wrap\ rate) \times (Pilots\ per\ aircraft) \times (t_{mission}) \tag{21}$$

$$Maintenance\ cost = (Mechanic\ wrap\ rate) \times (MMH/FH) \times (t_{mission}) \tag{22}$$

$t_{mission}$ is the mission time (including time spent on the ground), while MMH/FH is the number of maintenance man-hours required per flight hour. Values of 0.25-1 are typical for light aircraft [20].

Equation 21 assumes a piloted mission. If the mission is flown autonomously, the pilot cost model uses "bunker pilots" (pilots who remain in a control center on the ground, ready to provide assistance remotely if need be) instead [2]. Pilot cost is then instead computed using Equation 23:

$$Pilot\ cost = \frac{(Pilot\ wrap\ rate) \times (t_{mission})}{Aircraft\ per\ bunker\ pilot} \tag{23}$$

Energy cost is computed by multiplying the amount of electricity used during the mission by the price of electricity: $0.12 per kWh, the average price of electricity in the United States [2]. A 90% charging efficiency is assumed. Finally, indirect operating cost is estimated as a fixed 12% fraction of direct operating cost.

3. Effect of Deadhead

Some missions flown by the air taxi service will inevitably be deadhead missions: missions in which the aircraft is merely being repositioned for its next revenue-generating flight and no passengers are carried. In order to account for the effect of deadhead missions on cost, the aircraft is "flown" over both missions, and costs are computed for both.

The total cost of flying N_r revenue-generating missions at a cost c_r per mission and of flying N_d deadhead missions at a cost c_d per mission can be calculated using Equation 24:

$$Total\ cost = N_r c_r + N_d c_d \tag{24}$$

The cost per trip (including the effect of deadhead) is therefore calculated using Equation 26, obtained after some algebraic manipulation:

$$Cost\ per\ trip = \frac{Total\ cost}{N_r} = c_r + \frac{N_d}{N_r} c_d \tag{25}$$

$$Cost\ per\ trip = c_r + \frac{dr}{1 - dr} c_d \tag{26}$$

dr is the deadhead ratio: number of deadhead flights as a percentage of total number of flights.

4. Limitations

A number of important effects are not included in the cost model. For example, the same vehicle cost per unit empty weight is used for all configurations. This may not be an accurate assumption. For example, the lift + cruise configuration is aeromechanically quite simple as compared to configurations with more moving parts like the tilt wing and tilt rotor. It should therefore benefit from lower development, certification, and manufacturing costs, resulting in a reduced cost ratio. Taxes, insurance, landing fees, air traffic control (ATC) fees, and profit margin are all neglected by the cost model as well.

III. Results

In this section, a configurational trade study is presented, along with case studies, design requirements sensitivities, and vehicle parameter sensitivities.

A. Inputs

Input parameters are divided into two categories: generic inputs, for which the same value is used for all configurations; and configuration-specific inputs, where different values are used for each configuration. Generic input parameters are given in Table 7.

Table 7 Generic vehicle input parameters.

Parameter	Value
Battery specific energy	400 Wh/kg
Battery specific power	3 kW/kg
Vehicle autonomy enabled?	Yes

Mission parameters are given in Table 8. Inputs specific to the cost model were previously given in Table 5.

Table 8 Mission input parameters.

Mission	Sizing	Revenue	Deadhead
Mission type	Piloted	Piloted	Autonomous
Mission range	50 nmi	30 nmi	30 nmi
Number of passengers	3	2	0
Reserve type	FAA helicopter VFR	None	None

In practice, the deadhead mission cannot always be autonomous, as pilots will need to be relocated along with their aircraft in order to fly piloted revenue missions. Autonomous deadhead missions are used here to demonstrate the utility of the methodology; a sensitivity analysis is conducted as part of the case study on technology assumptions (Section III C 3).

Representative images of each configuration are shown in Figure 5.

(a) An example lift + cruise aircraft: the Aurora Flight Sciences prototype [23].

(b) An example compound helicopter: the Carter & Mooney SR/C [24].

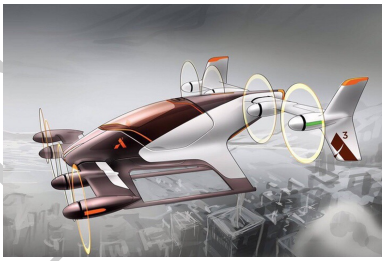

(c) An example tilt wing aircraft: the A^3 Vahana [25].

(d) An example tilt rotor: the Joby S2 [26].

(e) An example conventional helicopter: the Robinson R44 [27].

(f) An example coaxial helicopter: the Kamov Ka-32 [28].

(g) An example multirotor: the Ehang 184 [29].

(h) An example autogyro: the Magni M16 [30].

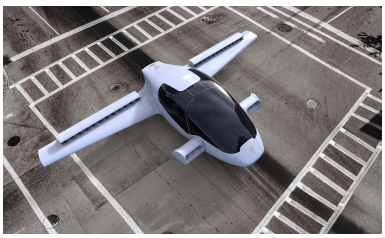

(i) An example tilt duct: the Lilium Jet [31].

Fig. 5 Configuration representative images. Note that the example conventional helicopter, coaxial helicopter, and autogyro are gasoline-powered; they do not represent eVTOL concepts.

Configuration-specific input data is given in Table 9. Cruising speed values were taken from Reference [4]. Reference [4] also gives a range of values for cruise lift-to-drag ratio and hover disk loading; the median values are used in this study. Values for number of rotors were taken from the vehicles in Figure 5.

As discussed in Section II A, a constant empty weight fraction is assumed for each configuration. A

recent study by Boeing [32] used configuration-specific structural, propulsion-system, and fixed-equipment weight models. Three eVTOL configurations were evaluated: a helicopter, a stopped rotor (lift + cruise), and a tilt rotor. Empty weight fraction estimates of 0.43, 0.53, and 0.55 were respectively obtained, and used here to estimate the values in Table 9.

As discussed in Section II A 3, rotor tip speed is a design variable. The optimizer tended to reduce the tip speed as much as possible, to reduce blade profile drag. Because the lower limit on tip speed is set by blade mean lift coefficient, understanding of this constraint is critical.

Helicopters typically operate with $\overline{C_l}$ between 0.3 and 0.6 [7]. This is because helicopters with higher values of $\overline{C_l}$ would be prone to retreating blade stall in forward flight. For this reason, $\overline{C_l}$ is constrained to below 0.6 for the conventional and coaxial helicopter.

Retreating blade stall is only an issue for configurations that use their rotors to provide lift in cruise. Therefore, configurations like the tilt rotor and lift + cruise, which do not use their rotors to provide lift in cruise, use a $\overline{C_l}$ constraint of 1.0. In theory, values as high as 1.5-1.6 could be used before the rotor stalls; the value of 1.0 provides a margin for control in hover. The compound helicopter uses its rotor to provide some (but not all) lift in cruise; a $\overline{C_l}$ constraint of 0.8 is used. The same value is used for the autogyro.

Table 9 Input data for each configuration [4].

Configuration	V_{cruise} (mph)	$\left(\frac{L}{D}\right)_{cruise}$	$\frac{T}{A}$ (lb/ft^2)	Empty weight fraction	$\overline{C_l}$ (upper limit)	N
Lift + cruise	150	10	15	0.53	1.0	8
Compound helicopter	150	9	4.5	0.5	0.8	1
Tilt wing	150	12	15	0.55	1.0	8
Tilt rotor	150	14	15	0.55	1.0	12
Conventional helicopter	100	4.25	4.5	0.43	0.6	1
Coaxial heli	150	5.5	7	0.43	0.6	2
Multirotor	50	1.5	3.75	0.43	0.6	8
Autogyro	100	3.5	3.75	0.5	0.8	1
Tilt duct	150	10	40	0.55	1.0	36

Although Table 9 includes parameter estimates for the autogyro and the tilt duct, they were not included in the trade study. This is because the vehicle performance model does not accurately describe these two configurations. For example, all three mission profiles include hover segments, but an autogyro is incapable of hover. Instead, the main rotor is unpowered, and autorotates in flight. Meanwhile, the tilt duct uses multiple ducted fans to provide lift in hover. These ducts provide an efficiency and noise benefit, relative to an unducted rotor [20]. In the absence of a model for taking these two benefits into account, the tilt duct was neglected.

The conventional and compound helicopters both have tail rotors, which consume additional power. The tail rotor of a typical helicopter consumes approximately 10-15% of the power consumed by the main rotor [7]. This adjustment can be applied to the conventional helicopter in both cruise and hover. However, the wing of a compound helicopter unloads the main rotor in cruise, causing it (and by extension, the tail rotor) to consume less power. As the wing and rotor power for the compound helicopter in cruise cannot be separated by the mission model, the additional power percentage applied to the compound helicopter was reduced.

Power increase assumptions for both configurations are given in Table 10.

Table 10 Power increase percentages for configurations with a tail rotor.

Configuration	Power increase (hover)	Power increase (cruise)
Conventional helicopter	15%	15%
Compound helicopter	15%	10%

Sound pressure level is computed during post-processing with the vehicle hovering 500 ft overhead (i.e. $z = \Delta S = 500\ ft$). This is in accordance with the Uber noise requirement (see Section II B 1).

B. Configuration Trade Study

1. *Results Overview*

A bar chart with some key results from the configurational trade study is shown in Figure 6.

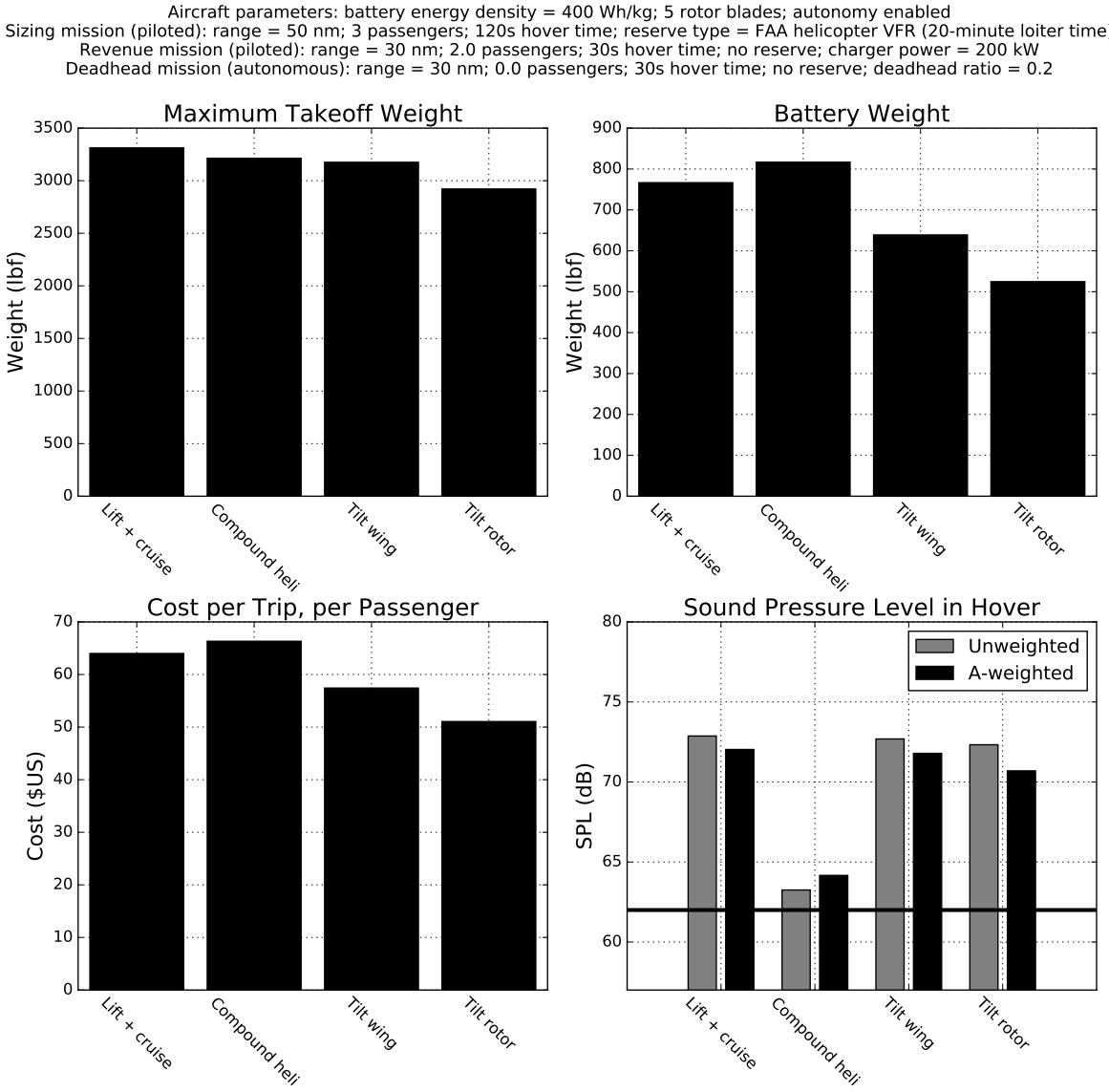

Fig. 6 Results of the configurational trade study. SPL values are from the sizing mission; the horizontal line represents the 62-dBA Uber noise requirement [2].

Several things are apparent from Figure 6. First of all, the multirotor, conventional helicopter, and coaxial helicopter are all missing. In the case of the multirotor, the optimizer returns Primal Infeasible; i.e. a solution for this configuration that satisfies all of the requirements and constraints does not exist. The conventional and coaxial helicopters do close, but at significantly higher weights: above 10,000 lbf and above 6,000 lbf respectively. Costs are also significantly higher. They were therefore dropped from consideration.

The four remaining configurations are the lift + cruise aircraft, the compound helicopter, the tilt wing, and the tilt rotor. These four configurations all have a relatively high lift-to-drag ratio, but also (with the exception of the compound helicopter) a relatively high disk loading. Since a high lift-to-drag ratio translates to increased efficiency in cruise, while a low disk loading translates to increased efficiency in hover, this means that cruise efficiency takes precedence over hover efficiency for the mission under consideration.

The sound pressure level varies widely between configurations, with unweighted values ranging from a low of about 63 dB for the compound helicopter to above 73 dB for the lift + cruise aircraft. A-weighting affects the results by at most 1-2 dB.

The compound helicopter is the most expensive configuration, but it is also the quietest. However, recall from Section II B 3 that tail rotor noise, potentially the dominant source of noise for this configuration, is neglected. Furthermore, no configuration is capable of meeting the 62-dBA Uber noise requirement. This indicates that vehicle noise is a critical issue for on-demand aviation.

Additional results from the configurational trade study are given in Figure 7.

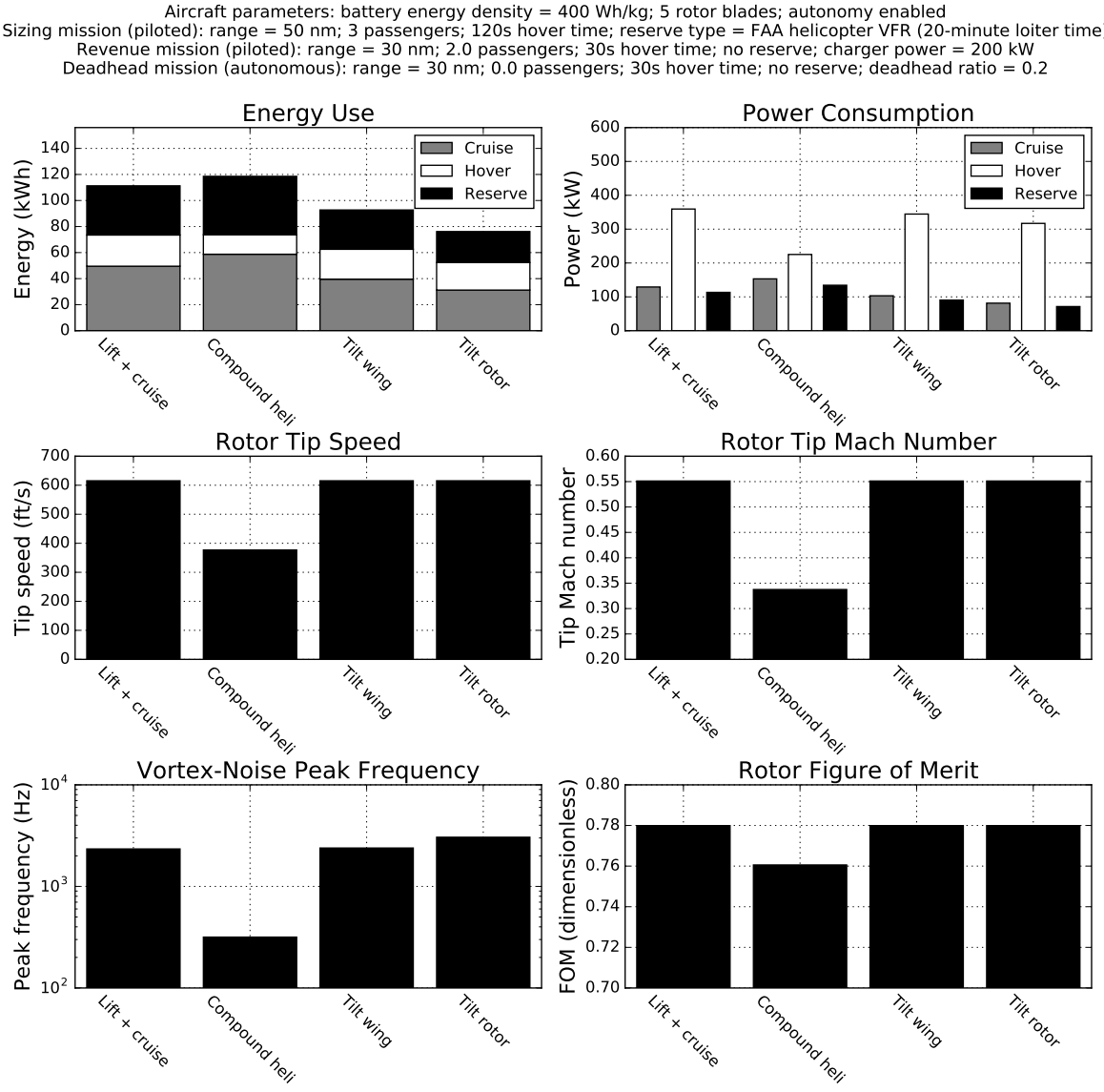

Fig. 7 More results from the configurational trade study. All data presented is from the sizing mission. Energy use in hover is the sum from all four hover segments.

Figure 7 shows that significant amounts of energy are consumed during all three categories of mission segment (cruise, hover, and reserve). Reserve power is lower than cruise power, due to the loiter adjustments discussed in Section II C. Also, all four aircraft consume significantly more power in hover than in cruise.

Helicopters may experience tip Mach numbers in forward flight approaching 0.9 [7]. Compressibility and thickness effects (which adversely impact both vehicle efficiency and noise) pose significant problems in

this regime. However, from Figure 7, rotor tip Mach numbers range from below 0.35 to slightly above 0.55. As discussed in Section II B 4, tip Mach effects are therefore not a problem for on-demand aircraft.

Note from Figure 6 that the compound helicopter actually becomes slightly louder if A-weighting is considered. This is because the compound helicopter has a vortex-noise peak frequency of about 300 Hz. It can be seen from Figure 4 that applying A-weighting to a sound at this frequency increases the sound pressure level. The other configurations have peak frequencies above 2,000 Hz; applying A-weighting therefore lowers the sound pressure level.

A cost breakdown is shown in Figure 8.

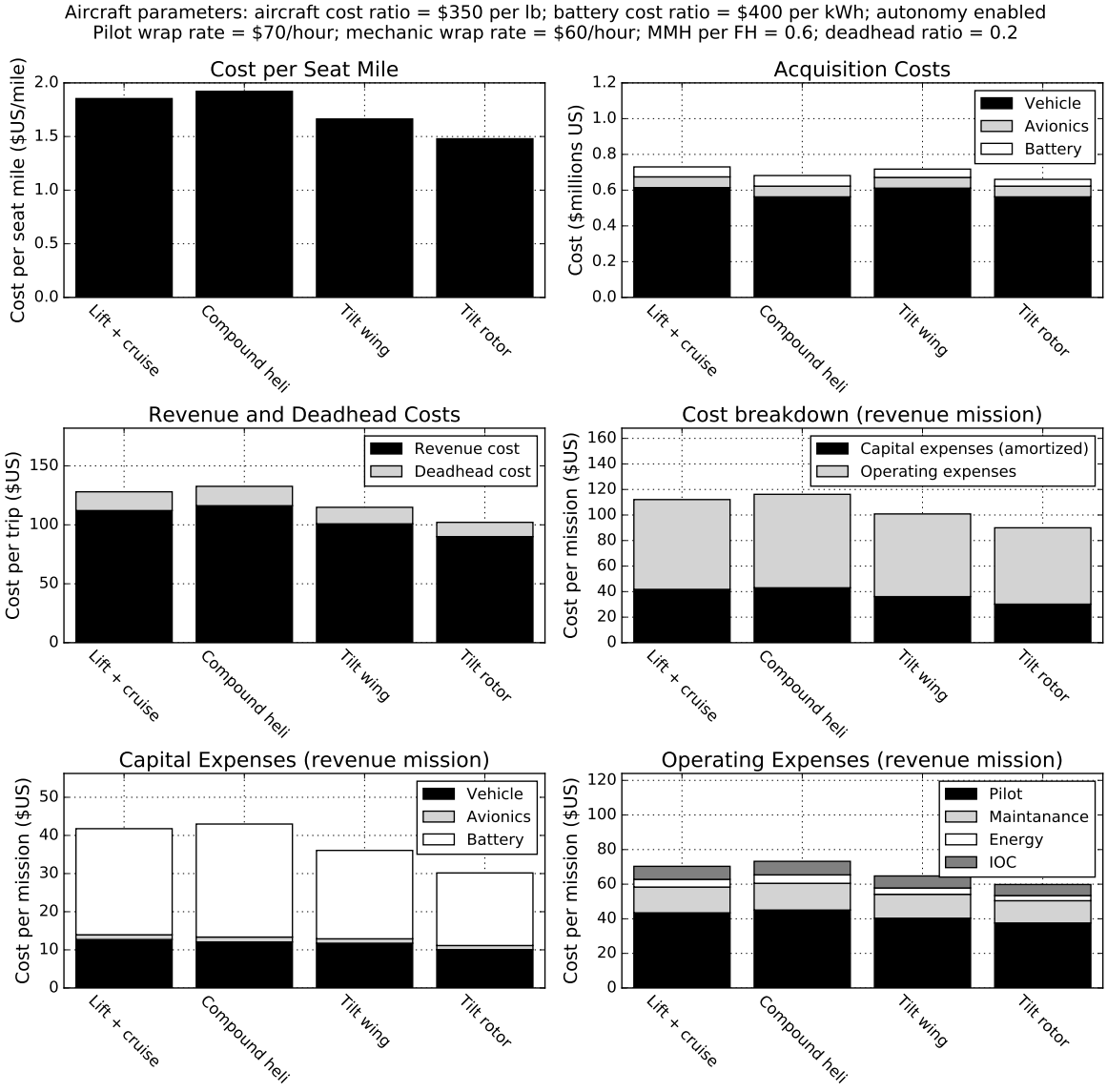

Fig. 8 Cost breakdown. Cost per seat mile is given in terms of statute miles, instead of nautical miles.

Figure 8 shows that cost per seat mile does not vary widely between configurations. Values range from as low as $1.50 per seat mile for the tilt rotor, to about $2.00 per seat mile for the compound helicopter. Operating expenses account for a somewhat larger share of revenue mission cost than capital expenses.

Interestingly, the deadhead mission cost is not very large as compared to the revenue-generating mission cost. This is partly because of the low deadhead ratio (Table 5); it is also because the deadhead mission is flown autonomously, with correspondingly lower pilot costs.

Despite the relatively small share of acquisition costs attributable to the battery, the battery accounts for a much larger share (about two-thirds) of amortized capital expenses. This is because the battery is amortized differently as compared to the vehicle and avionics. The latter two items are amortized using a 20,000 hour service life, while the battery is amortized using a 2,000-cycle life (i.e. 2,000 missions). Within operating expenses, pilot cost is dominant as compared to maintenance cost, energy cost, and indirect operating cost. Therefore, the keys to reducing the cost per trip are to 1) reduce battery manufacturing cost and increase cycle life (which lowers battery amortized cost) and 2) implement vehicle automation (which lowers pilot cost). This is discussed further in Section III C 3.

2. Noise Analysis

Example noise spectra, for an altitude $z = 500$ ft and observer ground location $y = 982$ ft, are presented in Figure 9. The resulting azimuthal angle is $\theta = 117°$. See Figure 3 for definitions of y, z, and θ. Only the first harmonic of rotational noise is shown; the other harmonics are negligibly small by comparison.

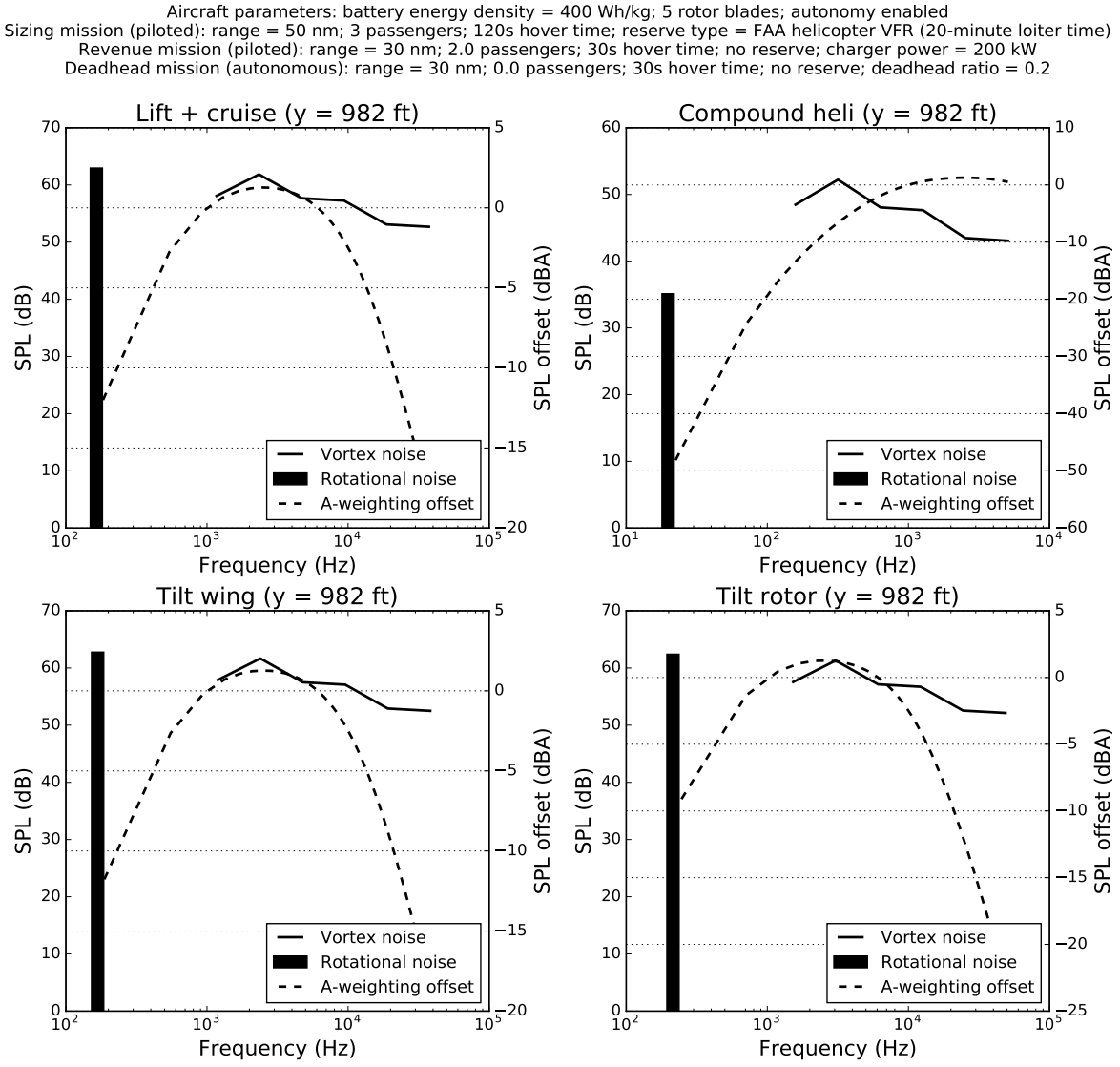

Fig. 9 Example noise spectra. Both rotational and vortex noise values are unweighted.

Figure 9 reveals that (with the exception of the compound helicopter) rotational and vortex noise are

comparable in magnitude. However, rotational noise occurs at a much lower frequency. The A-weighting frequency response function $A(f)$ is also plotted. Much of the vortex noise occurs in a regime between 1 and 7 kHz, where $A(f)$ is maximized. Meanwhile, rotational noise occurs at a much lower frequency, with a corresponding large negative weight. This suggests that A-weighted rotational noise is negligible for on-demand aircraft as compared to vortex noise.

A plot showing noise as a function of observer ground location y ($z = 500$ ft) is presented in Figure 10. Rotational noise values included the first 10 harmonics.

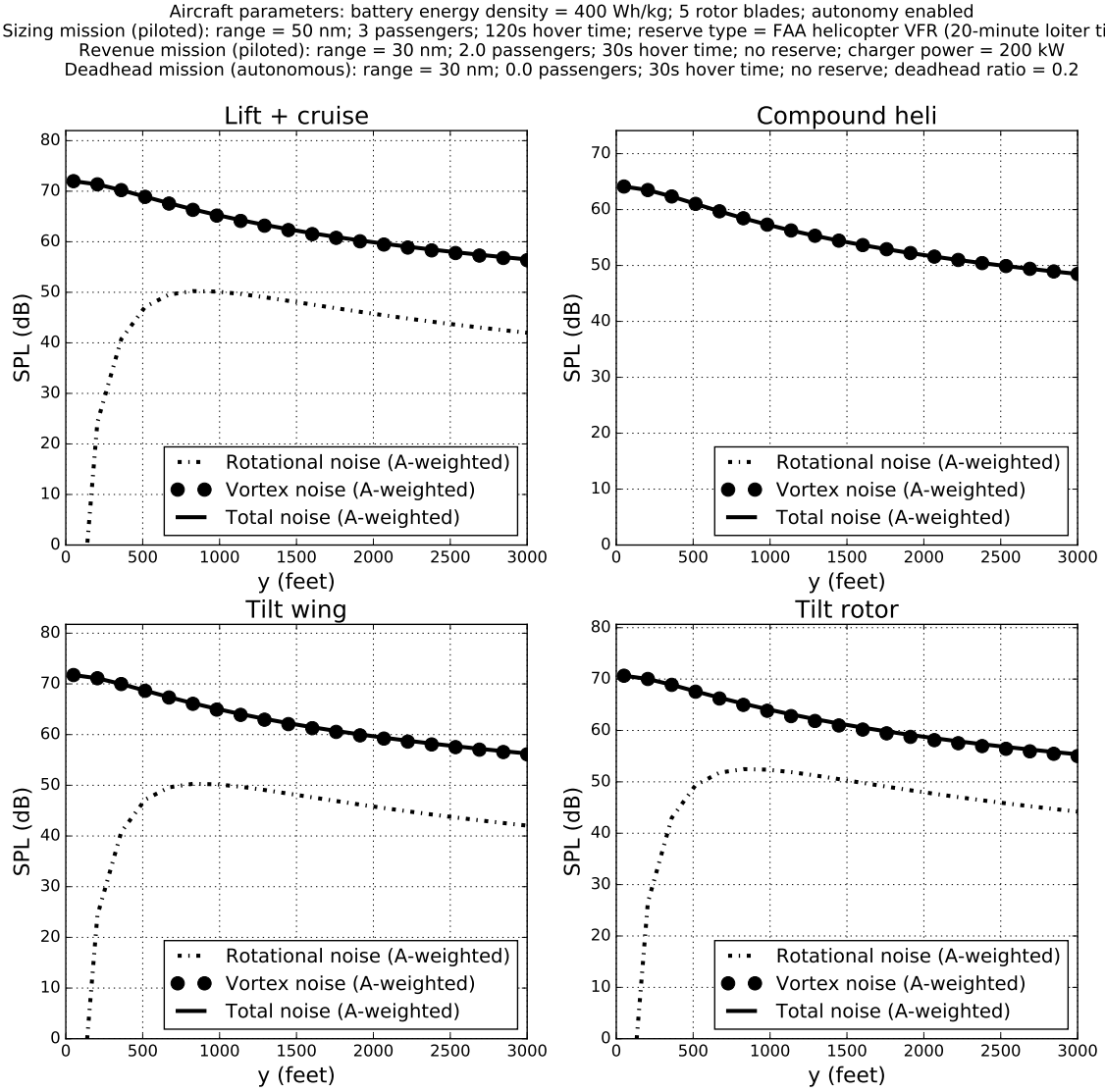

Fig. 10 Noise as a function of observer location, for constant $z = 500$ ft.

Figure 10 shows that A-weighted vortex noise dominates the spectrum for all values of y. Total noise (including both rotational and vortex noise) is plotted to show this more clearly. It can therefore be concluded from this section that rotational noise is negligible not just directly underneath the vehicle, but for all relevant observer positions while the vehicle is in hover. Also, because vortex noise is independent of azimuthal angle, noise directly underneath the vehicle at $z = \Delta S = 500$ ft is useful as a benchmark by which different vehicles can be compared.

C. Case Studies

1. *Sizing Plot*

Recall from Section III B that the compound helicopter is the most expensive configuration, but it is also the quietest. Table 9 shows that this configuration has the lowest cruise lift-to-drag ratio, but also the lowest disk loading. Therefore, a tradeoff between cruise and hover efficiency is hypothesized, depending on whether low cost or low noise is the priority. One way of illustrating this is with a carpet plot (hereafter called a sizing plot), in which optimized cost per trip and sound pressure level are plotted as a function of cruise lift-to-drag ratio and hover disk loading.

An example sizing plot is shown in Figure 11. Three configurations from Table 9, as well as two configurations from the aforementioned Boeing eVTOL study, are also shown. The Boeing lift + cruise configuration assumes a cruise lift-to-drag ratio of 9.1 and a disk loading of 7.3 lbf/ft^2; the Boeing tilt rotor assumes a cruise lift-to-drag ratio of 11.0 and a disk loading of 12.8 lbf/ft^2. These values were obtained from Reference [32]. Aside from these two parameters, all other assumptions are consistent with those previously described for the lift + cruise configuration.

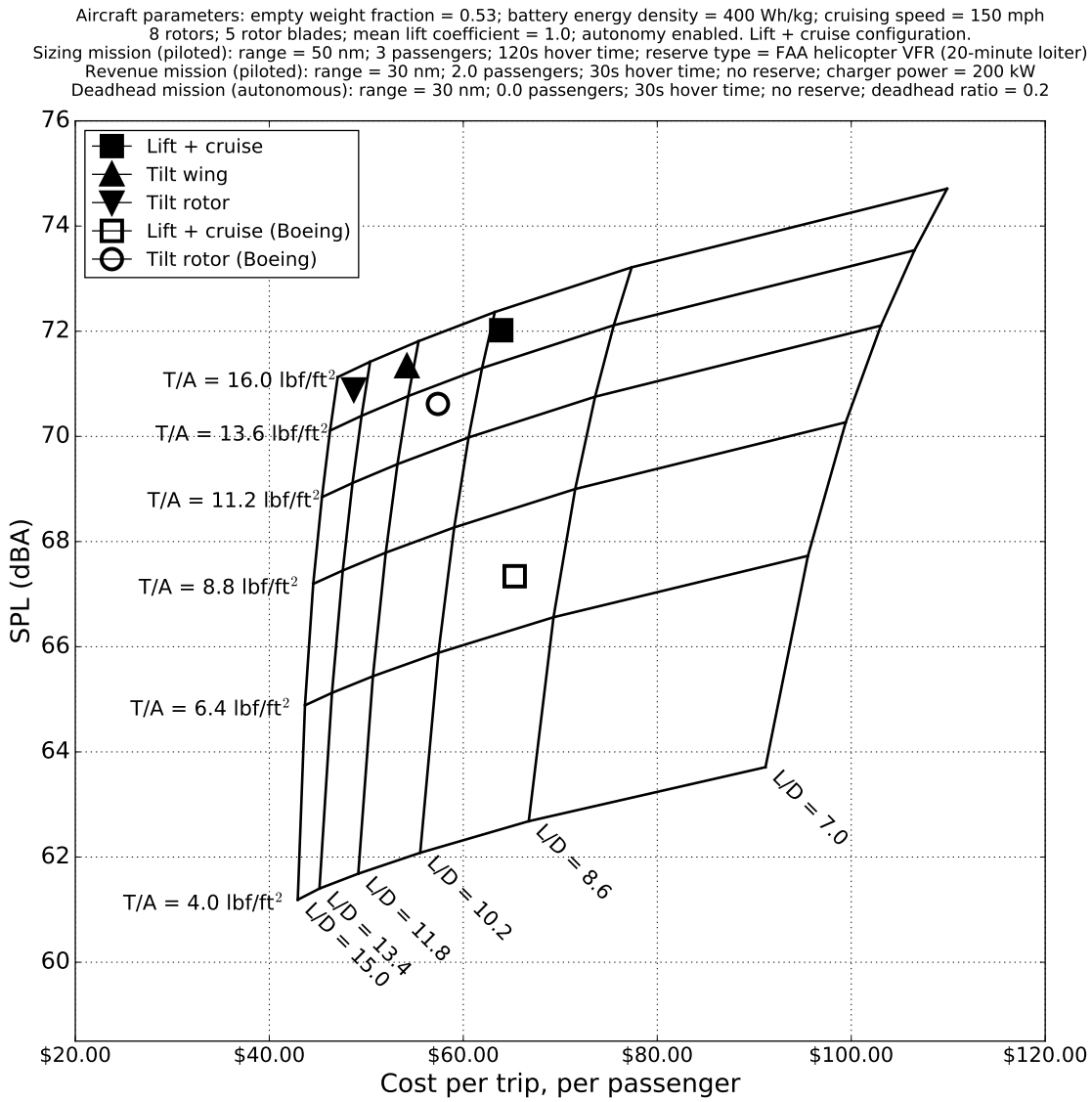

Fig. 11 Sizing plot for the lift + cruise configuration. An intersection between any two lines on the plot represents an optimized vehicle design, for that combination of cruise lift-to-drag ratio and hover disk loading.

Figure 11 shows that cost primarily depends on cruise lift-to-drag ratio; it is relatively insensitive to hover disk loading. However, the opposite is true for noise, implying that vehicle configuration selection may be driven by whether cost or noise is a primary requirement. As an example, take the tilt rotor and the Boeing lift + cruise configuration. The tilt rotor has a higher lift-to-drag ratio (14 vs. 9.1), which translates to lower power and energy requirements in cruise. This makes the tilt rotor significantly less expensive. However, the tilt rotor has a much higher disk loading (15 vs. 7.3 lbf/ft^2), resulting in greater noise.

The sizing plot is limited in the sense that it technically only applies to one configuration. While lift-to-drag ratio and disk loading can be varied, other inputs must be held constant. For example, the compound helicopter is not shown, because it has a lower empty weight fraction (Table 9) and greater power requirements due to its tail rotor (Table 10). The sizing plot is therefore better suited to making trades between similar configurations than to compare helicopters with winged vehicles. However, it does provide a simple yet powerful view of the eVTOL design space.

2. New York City Airport Transfers

New York City was selected as an example city in which to implement an on-demand aviation service. Air taxi services already exist in the city, provided by companies such as Blade [33] and New York Helicopter [34]. New York Helicopter provides airport transfer services between downtown helipads and local airports. Three downtown helipads are listed on their website: East 34th Street, West 30th Street, and Pier 6. Transfers are provided to three airports: John F. Kennedy (JFK), LaGuardia (LGA), and Newark (EWR).

The trip distance between each helipad and each airport was computed using Google Maps. Two sets of assumptions were used: a direct route, and an overwater-only route. As-the-crow-flies routes are generally not permitted in New York City. Instead, the city has defined routes that helicopters must follow. The direct route was selected as the shortest of the existing helicopter routes, as obtained from the maps in Reference [35].

The longest direct route is shown in Figure 12.

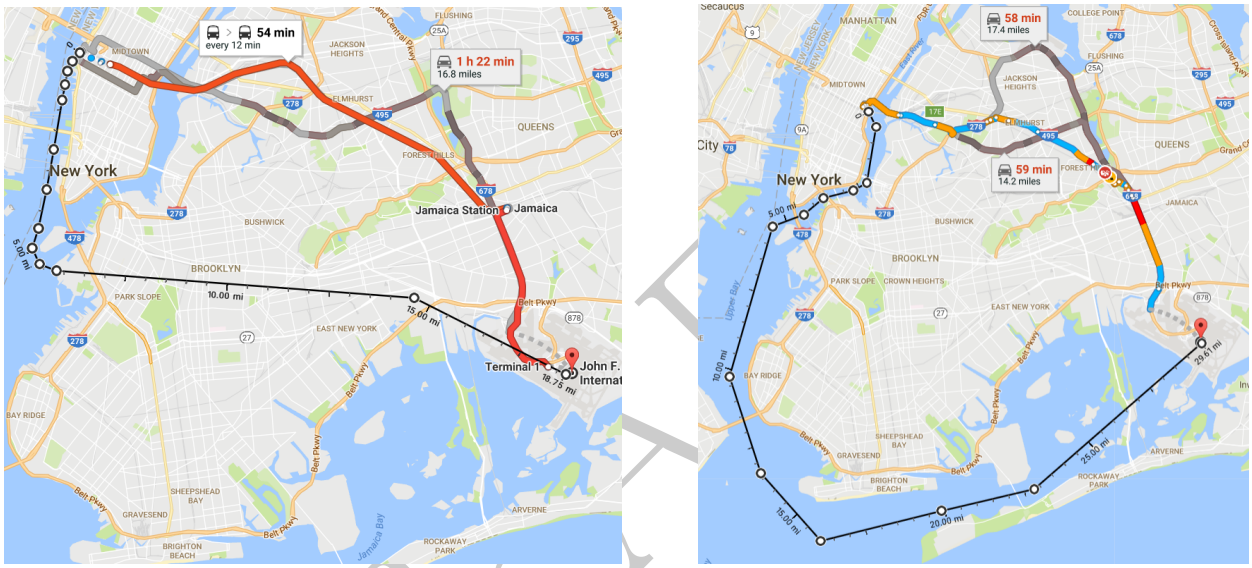

(a) The longest direct route: West 30th Street to JFK.

(b) The longest overwater route: East 34th Street to JFK.

Fig. 12 New York City helicopter routes (black lines). Note that the direct route passes over Brooklyn. While this is in accordance with the established helicopter route [35], an overwater-only route is also included in case this route is shut down for noise reasons.

Overwater-only routes were included in case on-demand aircraft are not permitted to fly over populated areas for noise reasons. Given the current controversy in New York City centered on noise generated by helicopter tour operators [12], overwater-only flights may become a necessity.

Computed trip distances are presented in Table 11. Note that in some cases, no direct route exists that is shorter than the overwater route. In these cases, direct and overwater route distances are identical.

The longest direct and overwater routes in Table 11 are West 30th Street to JFK (16.3 nmi) and East 34th Street to JFK (25.7 nmi) respectively. They are shown in Figure 12.

Based on Table 11, trip distances of 19 nmi for the direct flight and 30 nmi for the overwater flight were selected. A comparative study was conducted, using three sets of assumptions:

1. A 19 nmi sizing mission and a 19 nmi revenue mission. This corresponds to a vehicle that is solely capable of flying the direct route.

2. A 30 nmi sizing mission and a 19 nmi revenue mission. This corresponds to a vehicle that typically flies the direct route, but has the range to fly the overwater route if necessary.

3. A 30 nmi sizing mission and a 30 nmi revenue mission. This corresponds to a vehicle that always flies the overwater route.

Table 11 Trip distance for the airport transfer routes, computed using Google Maps.

Heliport	Airport	Distance (direct, nm)	Distance (overwater, nm)
West 30th Street	JFK	16.3	24.4
	LGA	14.2	14.2
	EWR	13.3	13.3
East 34th Street	JFK	9.9	25.7
	LGA	6.4	6.4
	EWR	14.3	14.3
Pier 6	JFK	10.3	21.7
	LGA	10.0	10.0
	EWR	10.6	10.6

The deadhead mission range is the same as the revenue mission range. Results are in Figure 13.

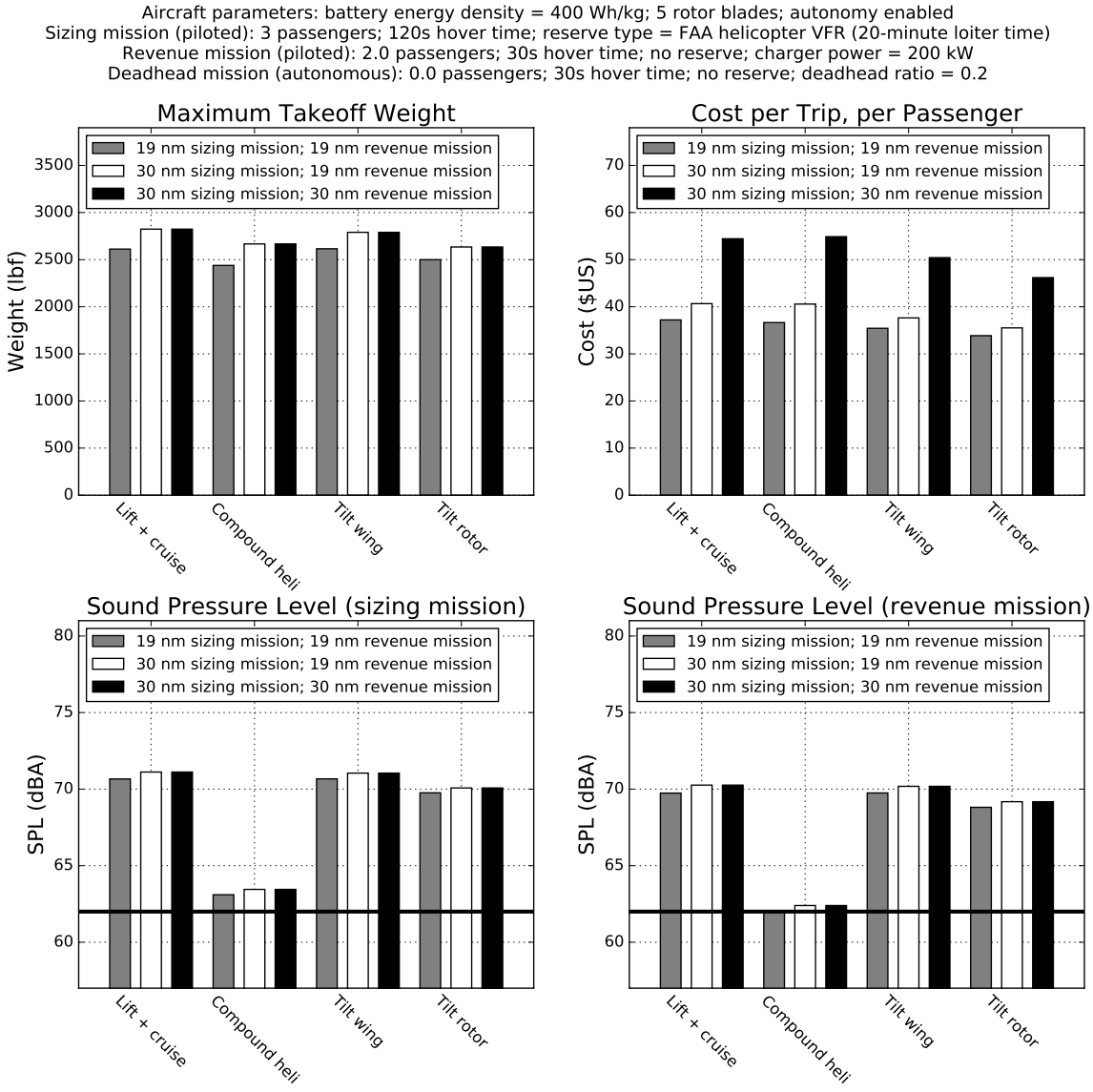

Fig. 13 Results from the New York City study.

Figure 13 shows that an on-demand electric air service will cost significantly less to operate than an equivalent helicopter service. The compound helicopter, the most expensive of the configurations in Figure 13, costs approximately $55 per passenger for an overwater flight. For comparison, New York Helicopter quotes a price of $1,900 per airport transfer, or $875 per passenger for a 2-passenger trip [34]. These two prices cannot be directly compared, as the New York Helicopter quote includes costs neglected by the model (see Section II D 4). However, an order-of-magnitude cost reduction illustrates that on-demand aviation has the potential to supplant existing services.

Vehicle weight and noise are not strongly affected by the mission assumptions. In particular, there is no difference between Options 2 and 3. However, the effect on cost per trip is much more significant. Flying a direct route results in substantial cost savings, even if the vehicle is sized to fly the overwater mission; this is mainly due to the reduced pilot and maintenance costs. Note that the noise level is somewhat lower during the revenue mission, as compared to the sizing mission. This is because fewer passengers are carried, resulting in a lighter aircraft.

As was noted in Section III B, the compound helicopter is the quietest configuration (if tail rotor noise is neglected), but is outperformed on cost. For this reason, a two-tiered service should be considered. Under such a model, compound helicopters can be used for flights over populated areas, where noise requirements are expected to be much more stringent. Other configurations can be used for overwater flights, where noise is less of a concern.

New York City would be a difficult place to roll out an on-demand air service, because the primary restrictions on market size are particularly acute there. Vascik and Hansman [36] identified three primary constraints on on-demand aviation market size: availability of ground infrastructure, interaction with air traffic control, and community acceptance of aircraft noise. New York City has some of the highest real-estate prices in the world, so obtaining space for additional helipads, charging stations, and maintenance facilities would be very expensive; with three large international airports and numerous smaller ones in the area, the airspace ranks among the world's busiest (second only to London); and community opposition to noise is already a major issue for the city's helicopter tour operators [12]. On-demand aviation operators must take these factors into account.

3. Technological Assumptions by Time Frame

Uber includes economic forecasts in their white paper, for three different time frames: initial, near term, and long term. They show that costs are strongly affected by the technological assumptions associated with each time frame. In this section, further investigations into this phenomenon are carried out.

Input parameters for each time frame are given in Table 12. Vehicle cost per unit empty weight ranges from business-jet levels at the high end, to current general-aviation levels at the low end (see Table 6). Battery cost per unit energy capacity is assumed to drop in accordance with US Department of Energy projections [2]. Deadhead ratios are reduced and use of autonomy is increased as on-demand aviation becomes more acceptable to consumers and regulators respectively, while battery specific energy is assumed to improve somewhat as well.

Table 12 Input parameters for the different time frames.

Time frame	Initial	Near term	Long term
Vehicle autonomy enabled?	No	Yes	Yes
Battery specific energy	400 Wh/kg	450 Wh/kg	500 Wh/kg
Sizing mission type	Piloted	Piloted	Piloted
Revenue mission type	Piloted	Piloted	Autonomous
Deadhead mission type	Piloted	Autonomous	Autonomous
Deadhead ratio	0.5	0.35	0.2
Vehicle cost ratio	$600 per lb	$400 per lb	$200 per lb
Battery cost ratio	$400 per kWh	$200 per kWh	$100 per kWh

Figure 14 contains an overview of the results.

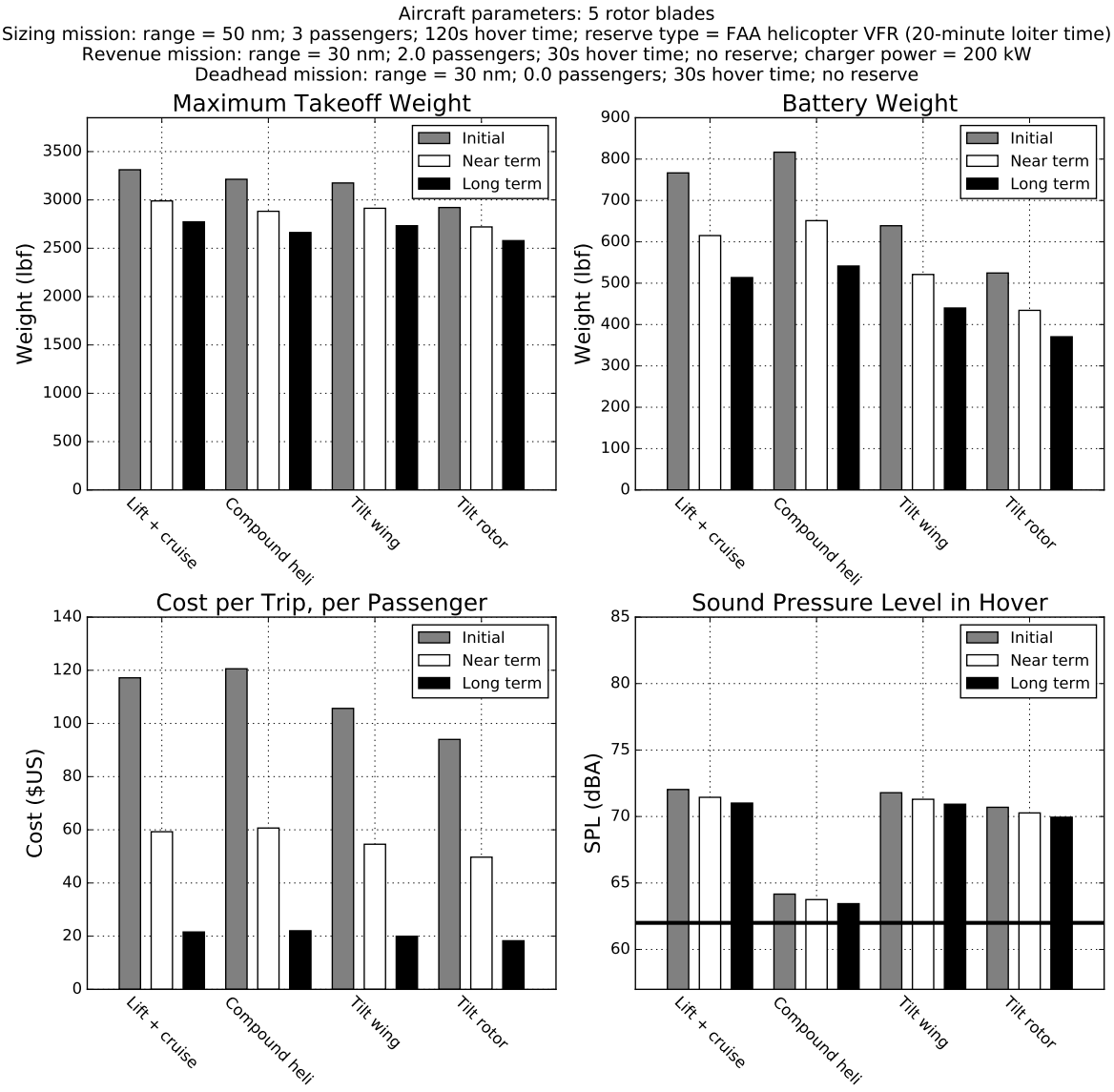

Fig. 14 Time frame study results.

Figure 14 shows that vehicle weight and battery weight decrease in accordance with technological assumptions associated with each time frame. Cost per trip decreases even more dramatically: by a factor of 5-6 between Initial and Long Term, depending on configuration. Recall from Section III B that the two main cost drivers are pilot salary and battery amortization. These costs are greatly reduced via vehicle automation and reduced battery manufacturing costs respectively.

However, the effect on noise is not nearly as large. Furthermore, even in the long term, no configuration is capable of meeting the Uber 62-dBA noise requirement. Therefore, a substantial amount of engineering effort should be expended on reducing vehicle noise, since simply relying on technology improvements will not suffice.

A cost breakdown is shown in Figure 15.

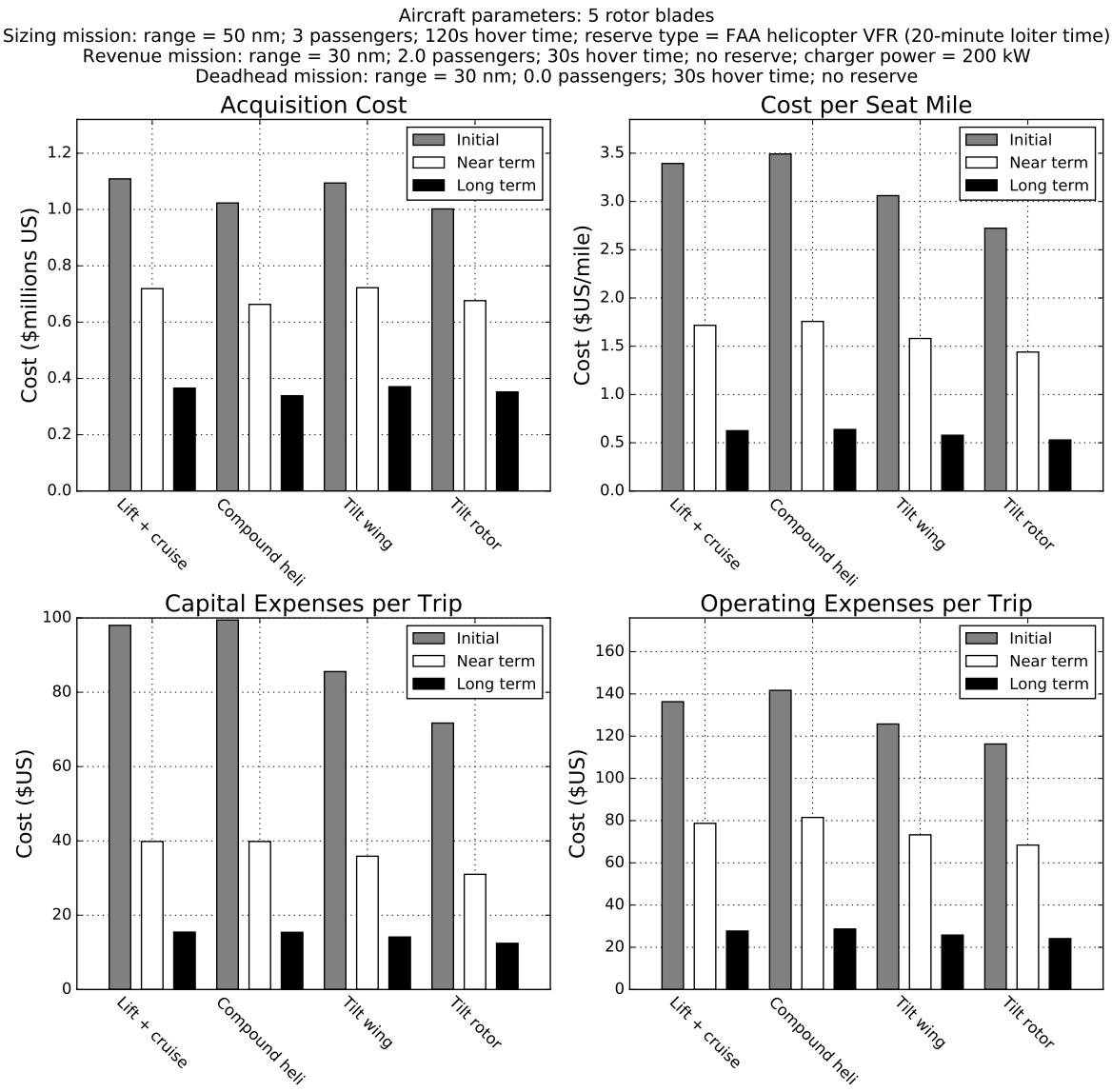

Fig. 15 Cost breakdown from the time frame study. Capital and operating expenses are per trip; i.e. the effect of deadhead is included. Cost per seat mile is given in terms of statute miles.

Figure 15 shows that all costs decrease substantially depending on the time frame assumption. In the case of the compound helicopter (the most expensive configuration), cost per seat mile decreases from almost $3.50 per mile initially, to as little as $0.60 per mile in the long term. For comparison, the average prices of UberX (car ridesharing, where the ride is paid for by one passenger) and UberPool (in which the ride is shared between multiple paying passengers) rides in the United States in 2016 were $2.34 per mile and $1.38 per mile respectively [2]. Recall again from Section II D 4 that a number of costs are neglected, so a direct comparison is not possible. However, it appears as if the proposed on-demand air service has the long-term potential to compete on price not just for expensive New York City airport transfers, but for everyday commutes as well.

4. Low-Noise Design

Five parameters were identified as having a significant impact on vehicle noise, without substantially affecting vehicle sizing: number of rotors, number of rotor blades, rotor solidity, blade thickness-to-chord ratio, and maximum mean lift coefficient. It was discovered during sensitivity analysis (not shown here) that number of rotors does not affect vehicle weight or cost, as long as disk loading is held constant. The goal of this case study is to investigate the design space formed by these five parameters, and try to determine combinations that reduce noise.

Three design categories were created. The first is the baseline, in which the same parameters from the configuration trade study (Section III B) are used. The second category is called Rotor Replacement. Here, the vehicle rotors are replaced with a different set, designed specifically for low noise. Only number of rotor blades and blade thickness-to-chord ratio are modified; rotor solidity is left unchanged. In the third category, called Aircraft Redesign, the entire vehicle is aggressively redesigned to reduce noise. All five identified parameters are modified.

The goal of the Rotor Replacement category is to design rotors that reduce noise, without affecting vehicle sizing. This requires a distinction to be drawn between the compound helicopter and the other configurations. Recall from Section III B that the compound helicopter has a vortex-noise peak frequency of around 300 Hz, below the value (600 Hz) at which the A-weighting response function is maximized. In this regime, reducing the peak frequency will decrease A-weighted sound pressure level. Towards this end, the number of blades was reduced from 5 to 3 (while holding solidity constant), and the rotor blade thickness-to-chord ratio was increased from 12% to 15%. Both changes have the effect of increasing the blade projected thickness, which in turn decreases the peak frequency (see Appendix D B).

The three other configurations have peak frequencies well above 600 Hz. In this regime, Figure 4 shows that the opposite rule applies: increasing the peak frequency will decrease A-weighted sound pressure level. Therefore, the number of blades was increased from 5 to 7, and the rotor blade thickness-to-chord ratio was decreased to 10%. Both changes have the effect of decreasing the blade projected thickness, which in turn increases the peak frequency. Note that this selection of blade count results in a blade aspect ratio of 22.3, which is quite high for a helicopter [7]. The resulting rotors may suffer from structural issues.

In the Aircraft Redesign category, a more aggressive approach is employed. The number of rotors is increased for all configurations except the compound helicopter. Although this does not affect vehicle weight, cost, or unweighted sound pressure level, it results in smaller rotors with correspondingly lower projected thicknesses. This in turn increases peak frequency.

Rotor mean lift coefficient is increased for all configurations. This results in a small benefit to vehicle weight and cost, but a large benefit to unweighted sound pressure level due to reduced tip speed (see the discussion in Section III A). However, it requires accepting smaller control margins in hover.

Finally, rotor solidity is increased to 0.14 for all configurations except the compound helicopter. This has a small, beneficial effect on vehicle sizing and a significant, beneficial effect on unweighted sound pressure level. (see Equation 15). Blade aspect ratio is maintained at a more-reasonable value of 15.9. Rotor solidity for the compound helicopter is unchanged, resulting in a reduced blade aspect ratio (9.6).

Parameter selections are summarized in Table 13.

Table 13 Input parameters for the low-noise design study. While the Aircraft Redesign category uses all five parameter values, the Rotor Replacement category only uses the values for number of rotor blades and blade thickness-to-chord ratio. Number of rotors, rotor solidity, and maximum mean lift coefficient for Rotor Replacement are the same as those from the configurational trade study.

Configuration	Number of rotors	Number of rotor blades	Rotor solidity	Rotor blade t/c	$\overline{C_l}$ (upper limit)
Lift + cruise	12	7	0.14	0.1	1.2
Compound heli	1	3	0.1	0.15	1.0
Tilt wing	12	7	0.14	0.1	1.2
Tilt rotor	16	7	0.14	0.1	1.2

Figure 16 contains an overview of the results.

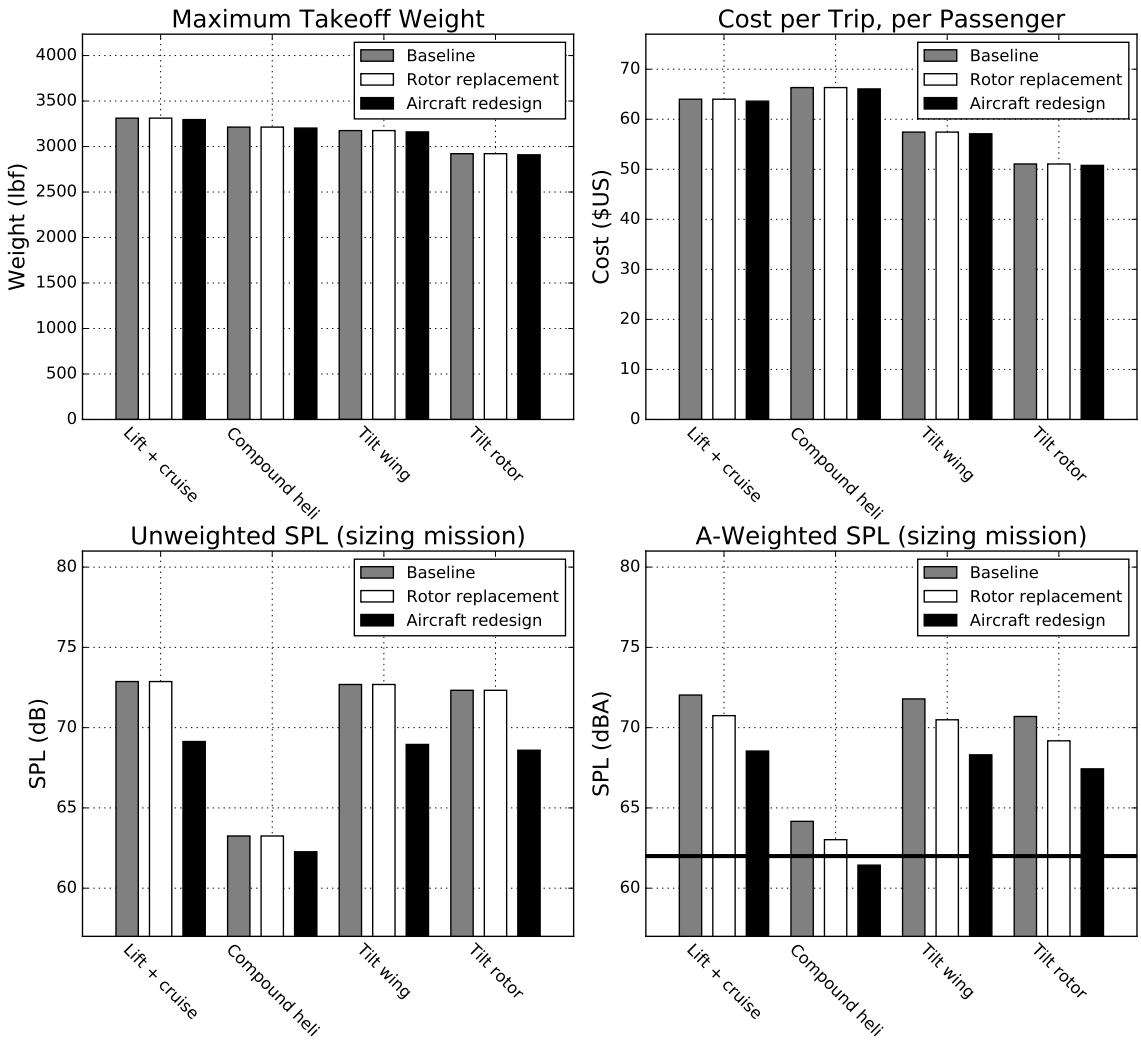

Fig. 16 First set of results from the low-noise design study.

Figure 16 shows that the Rotor Replacement strategy does not affect vehicle weight, cost, or unweighted sound pressure level. However, A-weighted sound pressure level is reduced by about 1 dBA on average. Meanwhile, the Aircraft Redesign strategy has a tiny, beneficial effect on weight and cost, but a significant effect on both unweighted and A-weighted sound pressure level. Therefore, while some noise benefits can be obtained by replacing the rotors, redesigning the aircraft with noise as a primary concern results in significantly larger reductions in noise.

Some design choices made as part of this design study may not be feasible. For example, a blade aspect ratio of 22.3 (used for the Rotor Replacement category) is very high for a helicopter. The feasibility of such a rotor must be verified using structural analysis.

Increasing mean lift coefficient and increasing rotor solidity both result in significant noise reductions, but the upper limit on these parameters is at present unclear. Mean lift coefficient is expected to be constrained by control margins in hover; additional analysis is required to determine the mean lift coefficient above which control margins cannot be maintained. Similarly, solidity is limited by blade interference; an upper limit is required.

Additional data is shown in Figure 17.

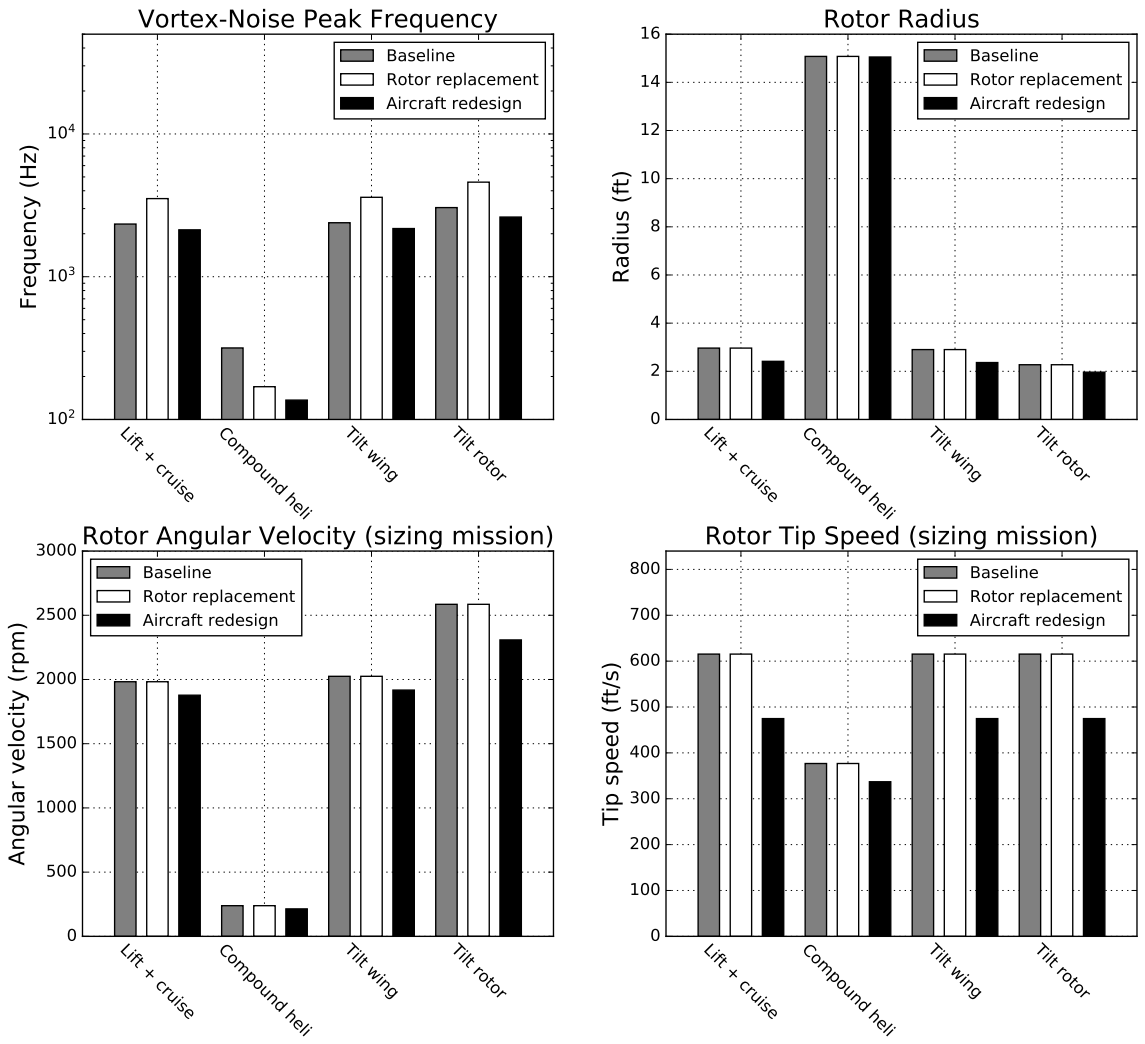

Fig. 17 Second set of results from the low-noise design study.

Figure 17 shows that the Rotor Replacement strategy produced the intended effect: vortex-noise peak frequency decreased for the compound helicopter, but increased for all other configurations. This was achieved without affecting rotor radius or tip speed, indicating that rotor replacement works as a drop-in solution for noise reduction. The Aircraft Redesign strategy results in more substantial design changes.

The only configuration that meets the 62-dBA noise requirement is the compound helicopter. This is only achievable with the Aircraft Redesign approach; also tail-rotor noise is neglected. Substantial engineering effort to reduce noise will therefore be required. A number of ideas for reducing noise were not investigated in this work, including: ducted rotors; swept, pointed, and/or split rotor blade tips; serrated rotor blade edges; and asynchronous blade design (used on the MacBook Pro cooling fan [37]). In addition, a number of new methods of reducing rotor noise are enabled by Distributed Electric Propulsion. Reference [38] cites two examples: motor digital control synchronization, and asynchronous RPM. These techniques should be investigated as part of a more detailed study.

D. Sensitivity Studies

In this section, the sensitivity of the optimized designs to various design requirements and vehicle parameters is explored. Each point on each plot represents an optimized design.

1. Mission Range

A sweep was conducted to determine the importance of mission range. The same range requirement is used for the sizing, revenue, and deadhead missions. Results are shown in Figure 18.

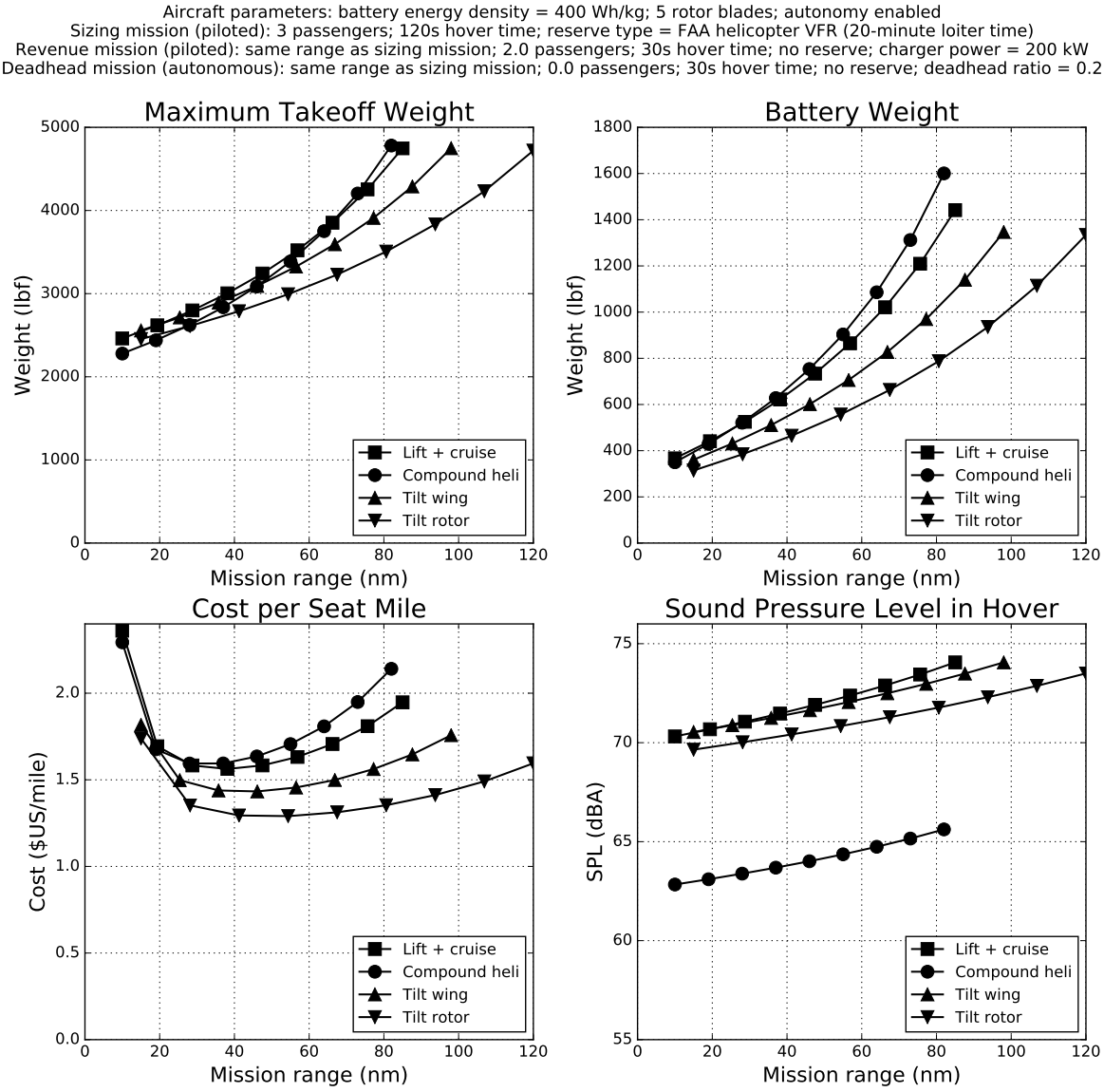

Fig. 18 Sensitivity to mission range. Cost per seat mile is plotted instead of cost per passenger.

Figure 18 shows that some configurations are more sensitive to mission range than others. The defining parameter input appears to be the cruise lift-to-drag ratio. The compound helicopter ($\frac{L}{D} = 9$, the lowest value) weighs and costs the most at longer ranges, while the tilt rotor ($\frac{L}{D} = 14$, the highest value) weighs and costs the least. Cost per seat mile is minimized at a mission range of about 30 nmi. On-demand aviation is at its most cost-competitive at this range; it may therefore be wise to use 30 nmi as a design requirement.

2. Number of Passengers

On-demand vehicle concepts produced by different companies vary in terms of number of passengers. For example, the A^3 Vahana carries one passenger and no pilot [25]. Meanwhile, the Uber white paper assumes a vehicle with four seats. If the vehicle is piloted, then three seats are available for passengers; all four seats can be occupied by passengers if the vehicle is autonomous [2].

A sweep was conducted to determine the importance of number of passengers carried on the sizing mission. The load factor was set to 2/3; i.e. the number of passengers carried on the typical mission was set equal to 2/3 times the number of passengers carried on the sizing mission. Results are shown in Figure 19.

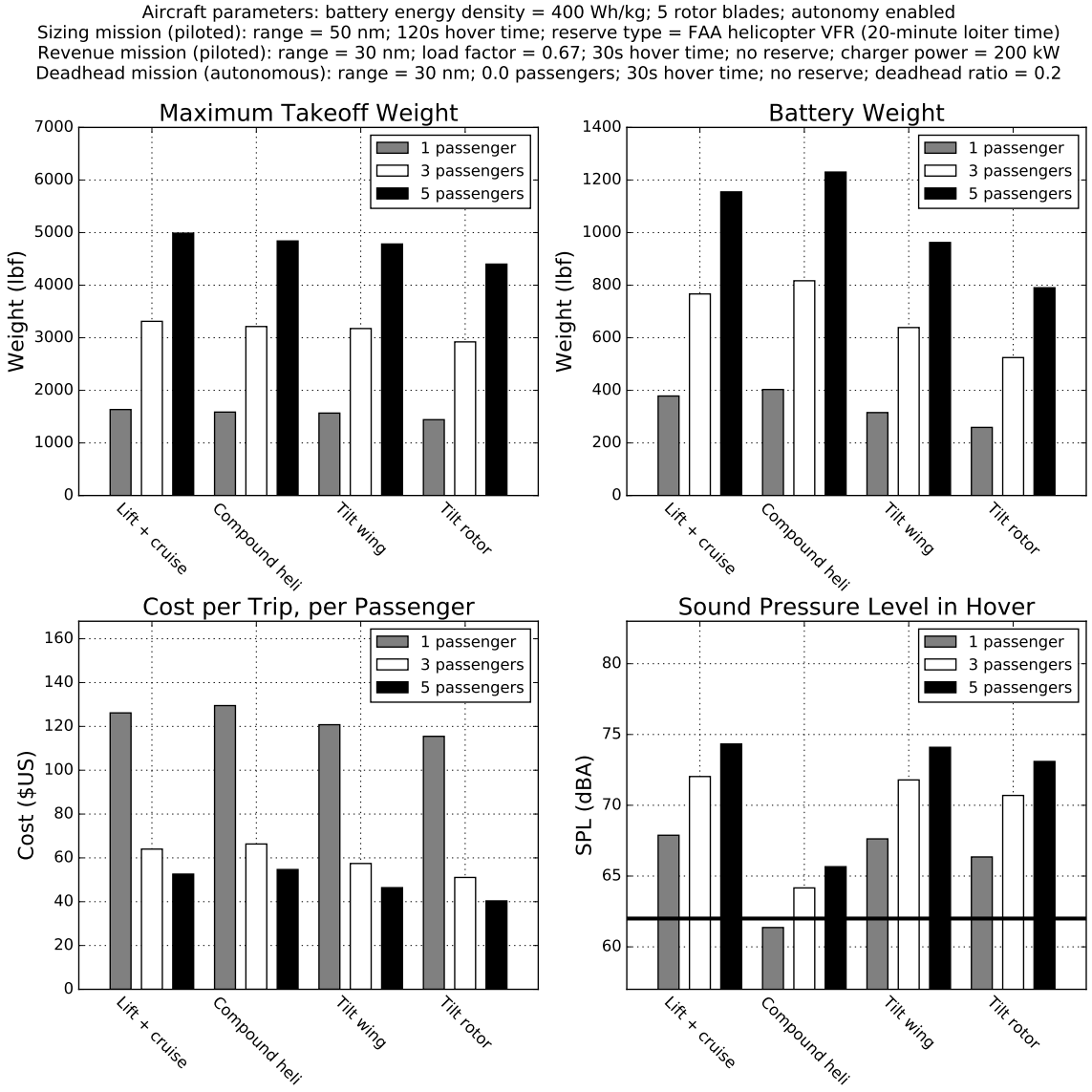

Fig. 19 Sensitivity to number of passengers carried on the sizing mission.

Figure 19 shows that weight and noise increase significantly with number of passengers. Cost per trip decreases, although diminishing returns are encountered beyond 3 passengers. Therefore, although 3 passengers seems reasonable, a decision on number of passengers must consider both cost and noise.

3. Reserve Requirement

On-demand aircraft companies are faced with a choice: should they certify their aircraft as airplanes or as helicopters? The FAA definitions are as follows [21]: "[airplane] means [a] fixed-wing aircraft...that is supported in flight by the dynamic reaction of the air against its wings", while "[helicopter] means [an] aircraft that depends principally for its support in flight on the lift generated by one or more rotors." For configurations with wings as well as rotors, either definition applies, and so a choice must be made.

From a certification perspective, the most important difference is in the reserve requirement: 30 minutes for airplanes vs. 20 minutes for helicopters (see Section II C). A study was conducted to determine the importance of this requirement. A 2-nmi diversion requirement was also included, in case a special regulatory class is created for eVTOL aircraft. Results are in Figure 20.

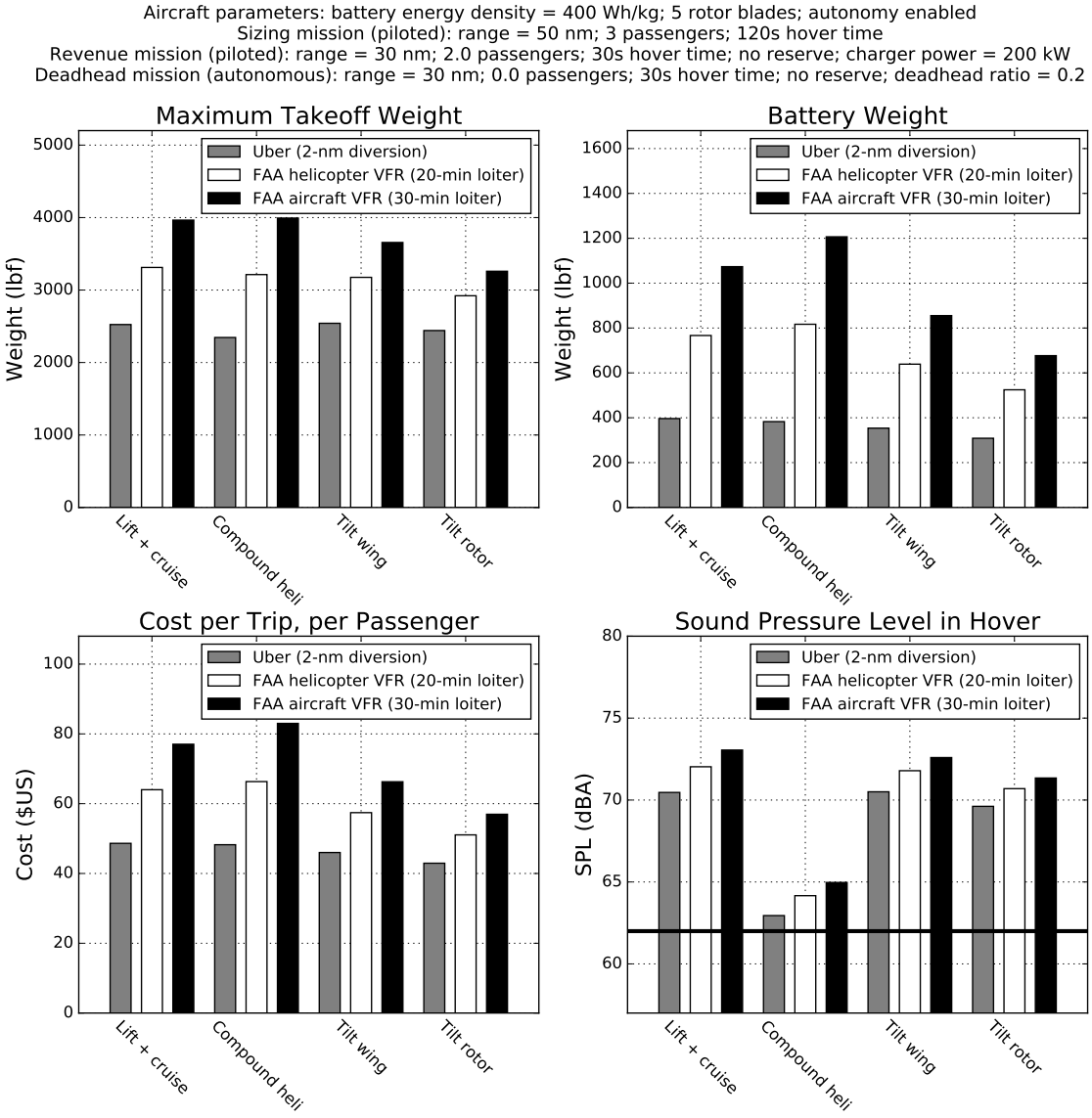

Fig. 20 Sensitivity to reserve requirement.

Figure 20 shows that the reserve requirement is critical. Vehicle weight, cost, and noise are all strongly affected. It seems as first glance that the logical choice is the helicopter requirement. This choice takes advantage of the existing certification framework, while providing a sizing benefit relative to the aircraft requirement. However, helicopter pilots are in short supply relative to aircraft pilots. In 2016, approxi-

mately 96,000 pilots held commercial ratings in the US; an additional 158,000 pilots held airline ratings [39]. By contrast, only 16,000 pilots held rotorcraft ratings. Barring full vehicle autonomy (impossible under current regulations), a pilot shortage would seriously impair the widespread adoption of on-demand aviation. Therefore, unless the regulations are changed, the choice of certification pathway should be carefully considered.

4. Battery Energy Density

A sweep was conducted to determine the importance of battery energy density. Results are shown in Figure 21.

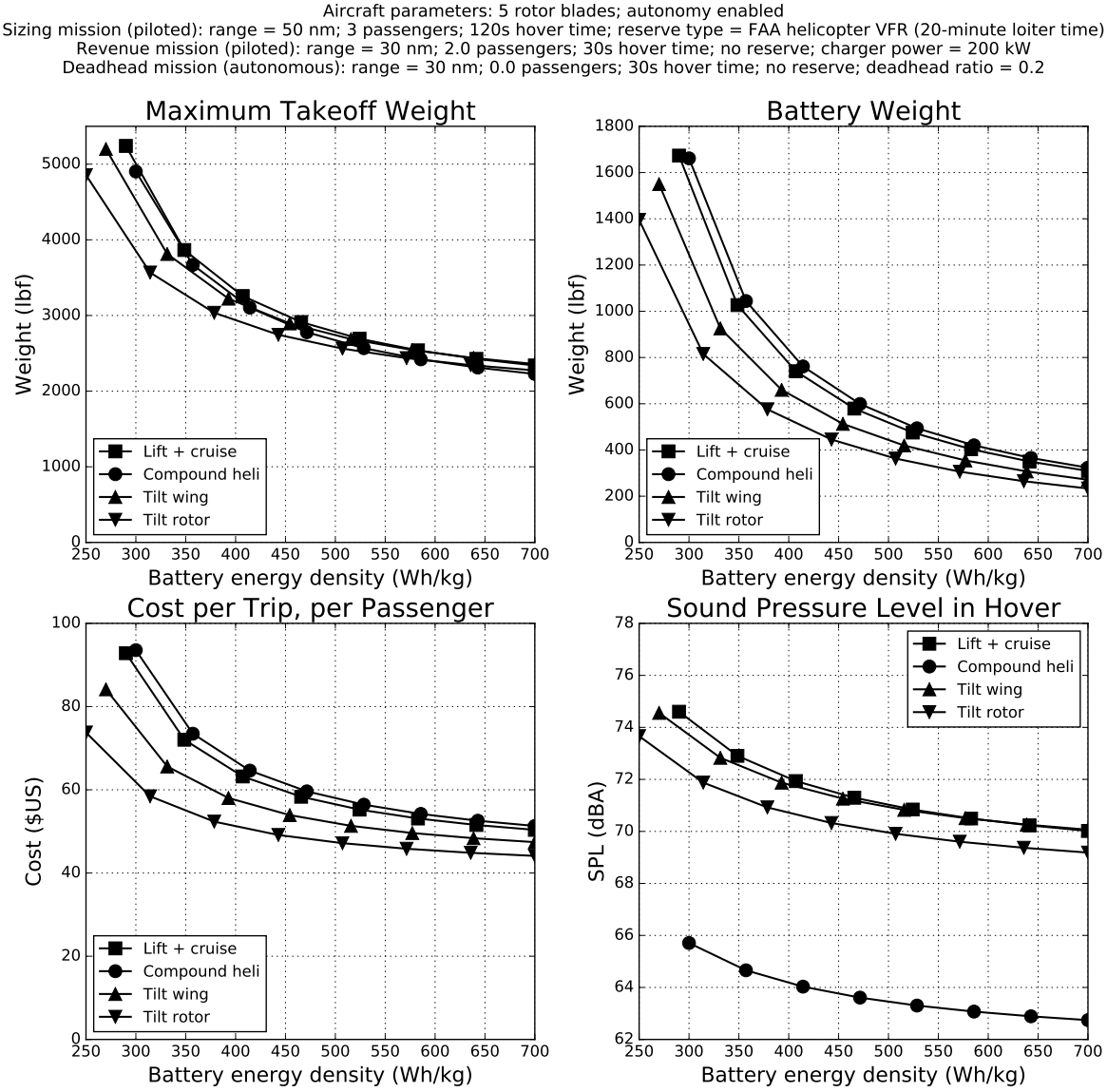

Fig. 21 Sensitivity to battery energy density.

Figure 21 shows that all four configurations are quite sensitive to battery energy density below around 400 Wh/kg, but less so above this point. Similar results have been obtained for other types of electric aircraft; ex. see Reference [38]. A battery energy density of 400 Wh/kg can therefore be seen as a critical enabling value for on-demand aviation.

IV. Future Work

Future work should primarily be focused on vehicle noise. It was shown in Section III C 3 that the 62-dBA Uber noise requirement cannot be met by any vehicle configuration, even with the most generous long-term technological assumptions. Vehicle noise is therefore a critical issue for on-demand aviation.

Noise research can be divided into four main areas. First of all, the noise model should be validated using higher-fidelity methods and/or experimental data. In particular, the value of the leading coefficient K_2 in Equation 15 for vortex noise was determined experimentally from helicopter data (see Appendix D A). K_2 is expected to vary between vehicle configurations. An accurate value for this parameter, for each configuration under examination, is required.

Secondly, it was hypothesized in Section II B 4 that blade slap can be avoided by careful selection of approach and departure procedures. While true for helicopters, this hypothesis must be verified for on-demand aircraft. The vortex ring state (which would result in a sudden, dangerous loss of lift) must also be avoided during approach and departure [7].

Thirdly, as discussed in Section II B 7, A-weighted sound pressure level is far from ideal as a noise metric, even for its stated goal of predicting human response to loudness. Furthermore, A-weighting cannot account for perceived annoyance. Examples of noise metrics designed to reflect annoyance include Perceived Noise Level (PNL) and Effective Perceived Noise Level (EPNL). EPNL is currently the standard metric for aircraft noise regulations [14], although its suitability for on-demand aviation has not been established. The use of PNL and EPNL, as well as the other noise metrics discussed in Section II B, should be explored.

Finally, a number of design opportunities for reducing noise were discussed in Section III C 4. However, the extent to which these opportunities can be exploited remains uncertain. Studies on rotor structural analysis (needed to limit blade aspect ratio), control margin requirements in hover (needed to limit rotor mean lift coefficient), and rotor blade interference (needed to limit rotor solidity) are required, in order to determine the extent to which noise can be reduced. Additional ideas for reducing noise (ex. ducted rotors, swept/pointed/split rotor blade tips, serrated rotor blade edges, asynchronous blade design, motor digital control synchronization, and asynchronous RPM) should also be explored.

V. Conclusions

A conceptual design and optimization tool for on-demand aviation was developed, using geometric programming. This tool was used to conduct a trade study between various aircraft configurations. For the selected mission, only four configurations are viable: the lift + cruise configuration, the compound helicopter, the tilt wing, and the tilt rotor. Configurations with a higher lift-to-drag ratio, but a higher disk loading, cost less to operate but are louder; carpet plots provide a valuable means of visualizing this tradeoff. The two most important costs are pilot salary and battery amortization; the key to lowering the price of on-demand aviation is therefore to implement vehicle autonomy and reduce battery manufacturing costs. The 62-dBA Uber noise requirement cannot be met by any vehicle configuration.

The New York City case study shows that an on-demand air service, even in the near term, is far superior in terms of price per trip as compared to current helicopter air taxi operations. Also, vehicle design may be impacted by design requirements specific to a given city. In the case of New York City, an overwater-only flight restriction, imposed for community noise reasons, would adversely affect costs and cannot be ignored by vehicle designers.

The case study on time frames shows that costs are strongly affected by technological assumptions. In particular, expected improvements in vehicle autonomy and battery manufacturing result in greatly reduced costs. In the long term, on-demand aviation becomes competitive with current car ridesharing services. This indicates the potential for on-demand aviation to become a commute system for the masses, as opposed to merely a high-priced service for the wealthy. However, the 62-dBA noise requirement is not met, even with the most generous long-term technological assumptions. This underscores the necessity of substantial engineering effort to reduce noise.

The case study on low-noise design shows that substantial opportunities exist for noise reduction. Five parameters were identified as having a strong effect on noise, without substantially affecting vehicle sizing: number of rotors, number of rotor blades, rotor solidity, blade thickness-to-chord ratio, and maximum mean

lift coefficient. A better knowledge of the limits on these parameters is required, in order to fully exploit the opportunities for noise reduction. While some noise benefits can be obtained merely by replacing the rotors, larger benefits are possible if the aircraft are redesigned with noise as a primary concern.

Vehicle weight, cost, and noise are strongly affected by all three design requirements for which sensitivity information was computed: mission range, number of passengers, and reserve requirement. Finally, a battery energy density of 400 Wh/kg was found to be a critical enabling value for on-demand aviation, a finding in accordance with the wider literature on electric aircraft.

Acknowledgments

The authors wish to thank all those who contributed their insights to this work. In particular, Parker Vascik, Edward "Ned" Burnell, Bjarni Kristinsson, Prof. Warren "Woody" Hoburg, and Prof. John Hansman of MIT; Carl Dietrich of Terrafugia; Martin Kearney-Fischer and Diana Siegel of Aurora Flight Sciences; Michael Duffy of Boeing; and Michel Merluzeau of AirInsightResearch; are acknowledged. The authors would also like to thank Ned and Prof. Hoburg for developing and maintaining GPkit, the open-source software package for solving geometric programs that was used throughout this research.

This work was funded in part by the Arthur Gelb graduate fellowship, and also by the AIAA William T. Piper, Sr. General Aviation Systems Graduate Award.

Appendices

A. Noise Definitions

Sound is a pressure wave; it consists of fluctuations in pressure in a medium. In air, pressure waves can be considered as follows [13]:

$$p_{total}(t) = p_0 + p(t) \tag{27}$$

$p_{total}(t)$ is the total air pressure, equal to the sum of the static (time-independent) pressure p_0 and the acoustic pressure $p(t)$. $p(t)$ is typically much smaller than p_0. For example, the standard-sea-level static pressure is approximately 100,000 Pa, while acoustic pressure is typically on the order of ± 1 Pa [13].

Effective sound pressure is the root-mean-square (RMS) value of the acoustic pressure $p(t)$. p is calculated by time-averaging over a period T, as shown in Equation 28:

$$p = \left[\frac{1}{T}\int_0^T p(t)^2 dt\right]^{1/2} \tag{28}$$

Sound pressure level is the most commonly used sound metric, and is abbreviated as SPL. It is calculated using Equation 29:

$$SPL = 10\log_{10}\left[\left(\frac{p}{p_{ref}}\right)^2\right] = 20\log_{10}\left(\frac{p}{p_{ref}}\right) \tag{29}$$

p_{ref}, the reference sound pressure, is typically set to 2×10^{-5} Pa. This represents the effective sound pressure at which an average adult can hear a 1 kHz tone [13].

B. Decibel Arithmetic

Obtaining the sum of two different sounds is not as simple as adding their respective sound pressure levels [13]. For example, the sum of two 60-dB sounds is not 120 dB. Instead, the laws of decibel arithmetic must be applied. The sum of n sounds, each with sound pressure level SPL_i, can be computed using Equations 30 and 31:

$$\left(\frac{p}{p_{ref}}\right)_i^2 = 10^{SPL_i/10} \tag{30}$$

$$SPL = 10\log_{10}\left[\sum_{i=1}^{n}\left(\frac{p}{p_{ref}}\right)_i^2\right] \tag{31}$$

Equation 31 only holds for independent, random sounds, or else sounds with different frequencies [13]. When adding multiple sounds with the same frequency, their relative phase must be considered.

C. Rotational Noise Derivation

As discussed in Section II B 5, rotational noise is divided into loading noise and thickness noise. The root-mean-square (RMS) sound pressures can be predicted using the classical Gutin and Deming formulae (Equations 32 and 33 respectively) [40]:

$$p_{m_L} = \frac{mB\Omega}{2\sqrt{2}\pi a(\Delta S)} \int_{hub}^{tip} \left[\frac{dT}{dr}\cos\theta - \frac{dQ}{dr}\frac{a}{\Omega r^2} \right] J_{mB}\left(\frac{mB\Omega}{a} r \sin\theta \right) dr \tag{32}$$

$$p_{m_T} = \frac{-\rho(mB\Omega)^2 B}{3\sqrt{2}\pi(\Delta S)} \int_{hub}^{tip} ctJ_{mB}\left(\frac{mB\Omega}{a} r \sin\theta \right) dr \tag{33}$$

p_{m_L} and p_{m_T} are the RMS sound pressures for loading and thickness noise respectively. m is the harmonic number, B is the number of rotor blades, Ω is the rotor angular velocity, a is the speed of sound, and ΔS is the distance between the rotor and the observer. T is the rotor thrust, Q is the rotor torque, r is the rotor radial location, and θ is the observer azimuthal location (see Figure 3). ρ is the air density, c is the blade chord, and t is the blade maximum thickness. J_{mB} is a Bessel function of the first kind of order mB.

The form of the Gutin and Deming formulae given in Equations 32 and 33 requires discretized values of rotor radius, thrust and torque. This form is used in Reference [40] in order to employ the outputs from blade-element analysis in acoustic calculations. However, in order to employ the simpler rotor model used in this work, an equivalent-radius approximation is used. All integrals are evaluated at an effective rotor radius R_e. The resulting alternate forms of the Gutin and Deming formulae are given in Equations 34 and 35 respectively:

$$p_{m_L} = \frac{mB\Omega}{2\sqrt{2}\pi a(\Delta S)} \left[T\cos\theta - Q\frac{a}{\Omega R_e^2} \right] J_{mB}\left(\frac{mB\Omega}{a} R_e \sin\theta \right) \tag{34}$$

$$p_{m_T} = \frac{-\rho(mB\Omega)^2 B}{3\sqrt{2}\pi(\Delta S)} ctR_e J_{mB}\left(\frac{mB\Omega}{a} R_e \sin\theta \right) \tag{35}$$

Once the loading and thickness pressures are known, sound pressure level SPL can be computed using Equation 36:

$$SPL = 10\log_{10}\left[\left(\frac{p_{m_L}^2 + p_{m_T}^2}{p_{ref}^2} \right) \right] \tag{36}$$

p_{ref} is the reference pressure, equal to 2×10^5 Pa.

Equation 36 only applies to one rotor. If multiple rotors are present, each operating under the same conditions, then Equation 31 must be employed. Therefore, the square of the pressure ratio is multiplied by the number of rotors N, resulting in Equation 37:

$$SPL = 10\log_{10}\left[N\left(\frac{p_{m_L}^2 + p_{m_T}^2}{p_{ref}^2} \right) \right] \tag{37}$$

As discussed in Appendix B, relative phase must technically be considered when adding multiple sounds with the same frequency. The technique used here assumes slightly different frequencies for each rotor; it serves as a reasonable first approximation. The propeller noise prediction method in SAE Standard 1407 [41] uses a similar technique.

D. Vortex Noise Derivation

A. Unweighted Sound Pressure Level

The vortex noise model used in this work was developed from the model in Schlegel et al. [19], as given in Reference [16]. Vortex noise in hover can be estimated using Equation 38, accurate to within ±2 dB of experimental data [16]:

$$SPL = 10\log_{10}\left(KA_b{V_{0.7}}^6\right) + 20\log_{10}\left(\frac{C_l}{0.4}\right) - 20\log_{10}\left(\frac{\Delta S}{\Delta S_{ref}}\right) \tag{38}$$

SPL is the sound pressure level at an observer distance ΔS from the source. K is a constant, equal to $6.1 \times 10^{-11}\ \frac{s^6}{ft^8}$. $V_{0.7}$ is the blade velocity at a radial location $r/R = 0.7$ (i.e. 0.7 times the tip speed). C_l is the local blade lift coefficient, referenced to $V_{0.7}$. ΔS_{ref} is equal to 300 ft.

Solve for the square of the pressure ratio using Equation 29 to obtain Equation 39:

$$\left(\frac{p}{p_{ref}}\right)^2 = KA_b{V_{0.7}}^6\left(\frac{C_l}{0.4}\right)^2\left(\frac{\Delta S_{ref}}{\Delta S}\right)^2 \tag{39}$$

Substitute the expression for blade area ($A_b = BcR$), and let $C_l = \overline{C_l}$. C_l is equal to $\overline{C_l}$ if constant downwash is assumed. This is a reasonable approximation, from Reference [7].

Once this approximation is made, combine Equation 3 (thrust coefficient) and Equation 11 (mean lift coefficient) to obtain Equation 40 for mean lift coefficient:

$$\overline{C_l} = 3\frac{C_T}{s} = \frac{6T}{\rho s V_T^2 A} \tag{40}$$

Substitute Equation 40 into Equation 39, substitute for tip speed ($V_{0.7} = 0.7V_T$), rearrange, and cancel terms to obtain Equation 41:

$$\left(\frac{p}{p_{ref}}\right)^2 = 0.7^6\left(\frac{6}{0.4}\right)^2 K\left(\frac{\Delta S_{ref}}{\Delta S}\right)^2 V_T^2\frac{T^2}{\rho^2 As} \tag{41}$$

The next step is to multiply by N, to account for the effect of multiple rotors. As with the rotational noise model (Appendix C), it is assumed that the rotors are operating at slightly different frequencies. Equation 31 can therefore be employed. We also combine the constants into one term: K_2.

$$K_2 = \sqrt{0.7^6\left(\frac{6}{0.4}\right)^2 K\left(\Delta S_{ref}\right)^2} \tag{42}$$

$$\left(\frac{p}{p_{ref}}\right)^2 = K_2^2\frac{V_T^2 N T^2}{\rho^2(\Delta S)^2 As} \tag{43}$$

The final result is Equation 44 for the sound pressure level:

$$SPL = 20\log_{10}\left[K_2\frac{V_T}{\rho(\Delta S)}\sqrt{\frac{NT}{s}\left(\frac{T}{A}\right)}\right] \tag{44}$$

Equation 44 was validated using data in Reference [19] for two different helicopter main rotors: the CH-3C and the CH-53A. Results are given in Figure 22. See Reference [19] for a more detailed description of the experimental setup.

Figure 22 shows that with an (experimentally determined) value of $K_2 = 1.206 \times 10^{-2}\ s^3/ft^3$, Equation 44 is accurate to within 3 dB of test data. This is technically only valid for the helicopters under consideration. Therefore, Equation 15 serves as a reasonable first approximation, and should also work for predicting noise trends. However, it is recommended in Reference [16] that K_2 be calibrated using higher-fidelity methods and/or experimental data for a given class of vehicle and/or experimental conditions.

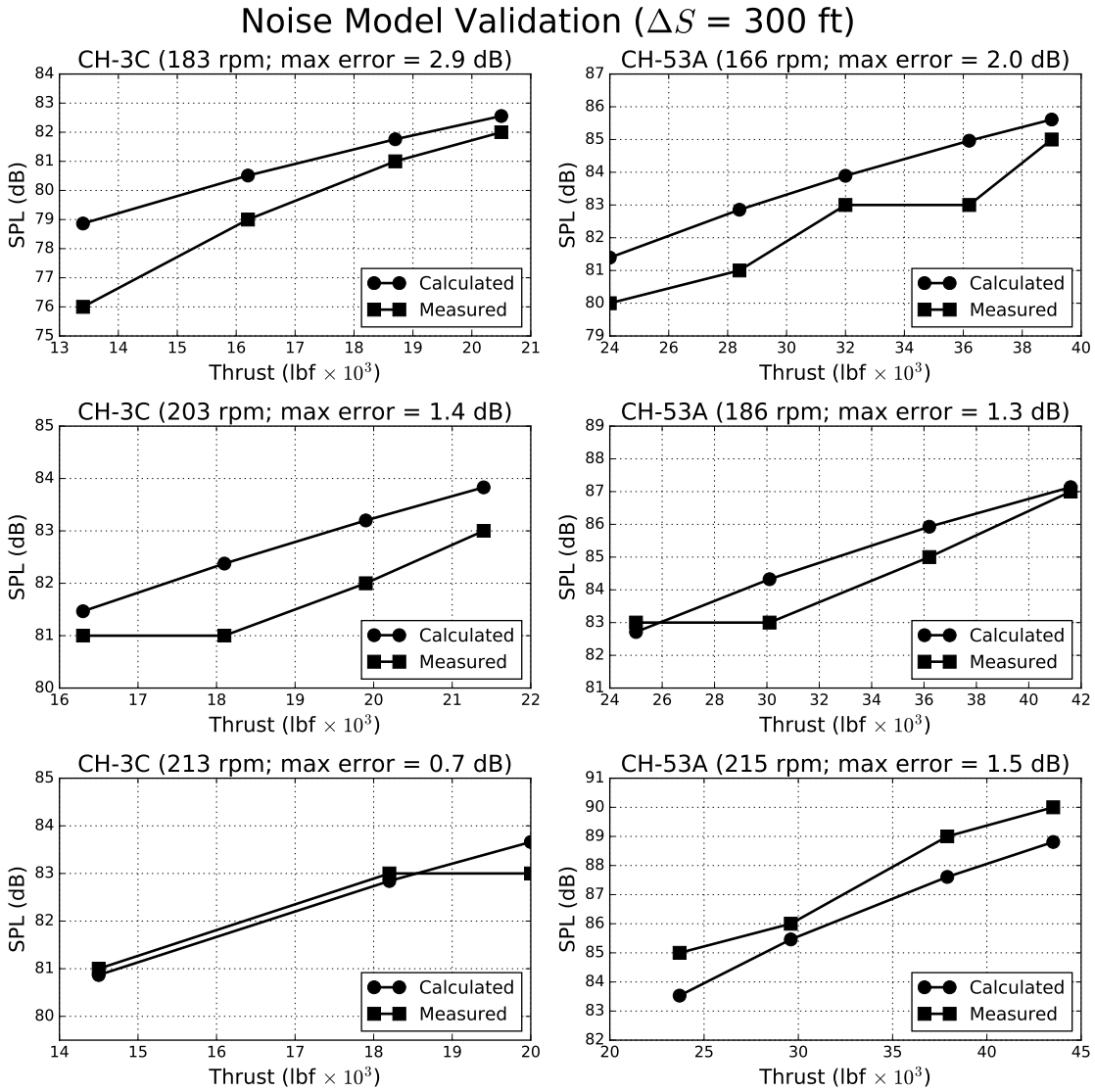

Fig. 22 Validation of the rotor vortex noise model. Note that the experimental data was rounded to the nearest decibel in Reference [19].

B. Frequency Spectrum

Although vortex noise is broadband in nature, it has a peak frequency (frequency at which the amplitude is highest). It can be estimated using Equation 45 [16]:

$$f_{peak} = \frac{(V_{0.7})St}{h} \tag{45}$$

f_{peak} is the vortex-noise peak frequency (in Hz), St is the Strouhal number, and h is the projected blade thickness. An estimate of $St = 0.28$ is used; this is a reasonable value for a helicopter [16]. h is computed using Equation 46:

$$h = t\cos\alpha + c\sin\alpha \tag{46}$$

t is the average blade thickness, α is the blade angle of attack (at $r/R = 0.7$), and c is the average blade chord. Two-dimensional airfoil theory is used to approximate the angle of attack:

$$\alpha = \frac{\overline{C_l}}{2\pi} \tag{47}$$

The blade chord is estimated using the definition of solidity (Equation 8). Since the NACA 0012 airfoil is a traditional choice for helicopter rotor blades [7], the blade thickness is calculated using an assumed thickness-to-chord ratio of 12%.

Once the peak frequency is known, the frequency spectrum can be drawn. Figure 23 shows the vortex-noise frequency spectrum for an unweighted sound pressure level of 0 dB. This figure was originally Figure 10 from Reference [16].

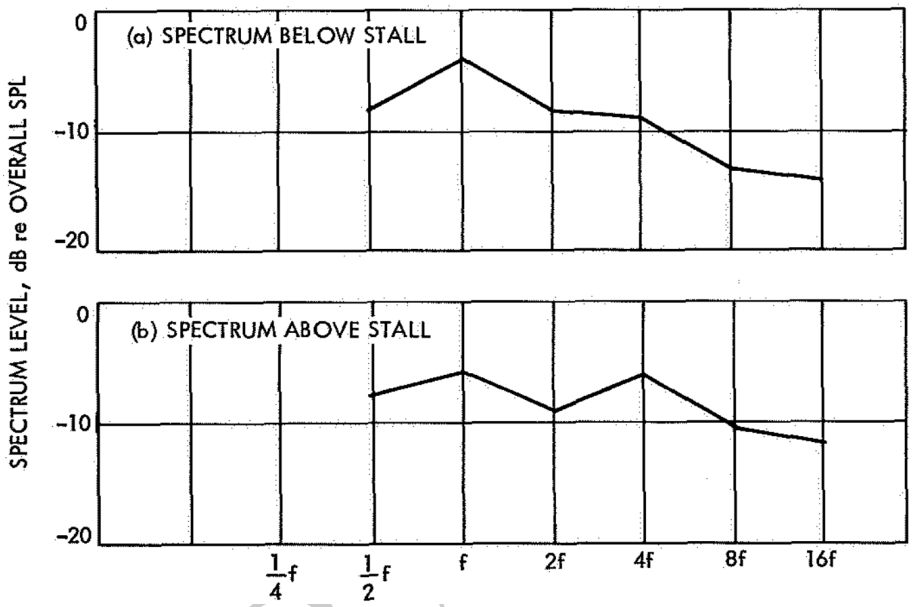

Fig. 23 Plot used to draw the vortex-noise frequency spectrum, obtained from Reference [16].

For each frequency value in Figure 23, the corresponding sound pressure level weight was obtained. Spectrum (a) is used, since it is assumed that the rotor is below stall. The weights are given in Table 14.

Table 14

Frequency	$\frac{1}{2}f_{peak}$	f_{peak}	$2f_{peak}$	$4f_{peak}$	$8f_{peak}$	$16f_{peak}$
SPL weight	7.92	4.17	8.33	8.75	12.92	13.33

The procedure for drawing the frequency spectrum is then as follows. First, calculate the overall SPL and peak frequency, using Equations 44 and 45 respectively. Then obtain the sound pressure level for each frequency in Table 14, by deducting the corresponding weight from the overall SPL. Finally, plot the resulting array of sound pressure level vs. peak frequency. Note that the interpolation between frequencies is only linear if the frequency axis uses a logarithmic scale.

C. A-Weighting Procedure

Because the frequency spectrum for vortex noise is continuous rather than discrete, the A-weighting technique for rotational noise discussed in Section II B 7 will not work. Instead, the approximate technique developed and used in this work replaces the summation in Equation 31 with an integral.

Recall from Figure 23 that the interpolated vortex-noise sound pressure levels are linear in log-space. Therefore, the sound pressure level in the interval between any two f-SPL pairs in Table 14 can be interpolated using Equations 48, 49, 50, and 51:

$$SPL = C_1 \log_{10}(fr) + C_2 \tag{48}$$

$$fr = \frac{f}{f_{peak}} \tag{49}$$

$$C_1 = \frac{SPL_2 - SPL_1}{\log_{10}(fr_2) - \log_{10}(fr_1)} \tag{50}$$

$$C_2 = SPL_2 - C_1 \log_{10}(fr_2) \tag{51}$$

fr is the frequency ratio; it is introduced in order to render the interpolation dimensionless. C_1 and C_2 are interpolation constants, while the pairs (fr_1, SPL_1) and (fr_2, SPL_2) represent the frequency-sound pairs defining the upper and lower limits on the interpolation interval under consideration.

According to the laws of decibel arithmetic, adding sounds of different frequencies is analogous to adding the squares of the RMS sound pressure ratios. Therefore, the goal is to obtain the sound pressure ratio, and integrate it over each frequency interval. Writing Equation 48 in terms of pressure ratio yields Equation 53:

$$SPL = C_1 \log_{10}(fr) + C_2 = 10 \log_{10} \left[\left(\frac{p}{p_{ref}} \right)^2 \right] \tag{52}$$

$$\left(\frac{p}{p_{ref}} \right)^2 = 10^{\frac{C_2}{10}} fr^{\frac{C_1}{10}} \tag{53}$$

Integrating over the interval and assuming $C_1 \neq -10$ yields Equation 54:

$$\int_1^2 \left(\frac{p}{p_{ref}} \right)^2 = 10^{\frac{C_2}{10}} \left. \frac{fr^{\frac{C_1}{10}+1}}{\frac{C_1}{10}+1} \right|_{fr_1}^{fr_2} \tag{54}$$

Finally, the total sound pressure level over $n-1$ intervals can be computed using Equation 55:

$$SPL = 10 \log_{10} \left(\sum_{i=1}^{n-1} \left[\int_1^2 \left(\frac{p}{p_{ref}} \right)^2 \right] \right) \tag{55}$$

The procedure for obtaining the A-weighted vortex-noise sound pressure level can be summarized as follows:

- Obtain the peak frequency and the frequency spectrum array, as described in Appendix D B.
- Apply the A-weighting offset function $A(f)$ to each sound pressure level in the frequency spectrum array.
- For each frequency in the spectrum array, obtain the corresponding frequency ratio using Equation 49.
- For each interval in the spectrum array, obtain the constants C_1 and C_2 using Equations 50 and 51 respectively.
- For each interval in the spectrum array, solve for the pressure ratio integral using Equation 54.

- Obtain the total A-weighted sound pressure level by adding the pressure ratio integrals using Equation 55.

Ideally, if step 2 is skipped (i.e. if A-weighting is not applied), then the resulting sound pressure level should be identical to that obtained from Equation 44. However, due to the approximations made in drawing the frequency spectrum, the obtained answer is approximately 1.3 dB higher than that predicted by Equation 44. This technique is therefore somewhat conservative.

References

[1] Moore, M. D., "Concept of Operations for Highly Autonomous Electric Zip Aviation," Conference Paper, 14th AIAA Aviation Technology and Integration and and Operations (ATIO) Conference, 2012.

[2] Holden, J. and Goel, N., "Fast-Forwarding to a Future of On-Demand Urban Air Transportation," White Paper, Uber, 2016.

[3] "Uber Elevate: Fast-Forwarding to the Future of On-Demand, Urban Air Transportation," `https://www.uber.com/info/elevate/summit/`, 2017.

[4] McDonald, R. and German, B., "eVTOL Stored Energy Overview," Presentation Slides, 2017. Uber Elevate summit.

[5] Hoburg, W. and Abbeel, P., "Geometric Programming for Aircraft Design Optimization," *AIAA Journal*, Vol. 52, No. 11, 2014, pp. 2414–2426.

[6] Burton, M. J. and Hoburg, W. W., "Solar-Electric and Gas Powered, Long-Endurance UAV Sizing via Geometric Programming," Conference Paper, AIAA AVIATION Forum, Denver, CO, 2017.

[7] Seddon, J. and Newman, S., *Basic Helicopter Aerodynamics*, John Wiley & Sons, 3rd ed., 2011.

[8] Bagai, A. and Leishman, J. G., "Experimental Study of Rotor Wake/Body Interactions in Hover," *Journal of the American Helicopter Society*, Vol. 37, No. 4, 1992, pp. 48–57.

[9] Leishman, J. G., *Principles of Helicopter Aerodynamics*, Cambridge University Press, New York, NY, 2nd ed., 2006.

[10] Woolhouse, M., "Officials will study plane noise after complaints about Logan," `https://www.bostonglobe.com/business/2016/10/07/faa-massport-agree-study-airplane-noise-after-rising-complaints/hIVSjqJnk5vwv6gAHzk0eI/story.html`, 2016.

[11] Choi, S., Alonso, J. J., and Kroo, I. M., "Multifidelity Design Optimization of Low-Boom Supersonic Jets," *Journal of Aircraft*, Vol. 45, No. 1, 2008, pp. 106–118.

[12] Moorman, R. W., "Noise In the Cities - Revisited," *Vertiflite*, 2016.

[13] Fahy, F. and Thompson, D., *Fundamentals of Sound and Vibration*, CRC Press, Taylor & Francis Group, Boca Raton, FL, 2nd ed., 2015.

[14] Zaporozhets, O., Tokarev, V., and Attenborough, K., *Aircraft Noise: Assessment, Prediction, and Control*, CRC Press, Taylor & Francis Group, Boca Raton, FL, 2011.

[15] Lowson, M. and Ollerhead, J., "A Theoretical Study of Helicopter Rotor Noise," *Journal of Sound and Vibration*, Vol. 9, No. 2, 1969, pp. 197–222.

[16] Marte, J. E. and Kurtz, D. W., "A Review of Aerodynamic Noise from Propellers, Rotors, and Lift Fans," Technical Report 32-1462, Jet Propulsion Laboratory, Pasadena, CA, 1970.

[17] "Fly Neighborly Guide," Technical Report, Helicopter Association International, Alexandria, VA, 2013.

[18] Johnson, W., *Helicopter Theory*, Dover Publications, New York, NY, 1994.

[19] Schlegel, R., King, R., and Muli, H., "Helicopter Rotor Noise Generation and Propagation," Technical Report, US Army Aviation Material Laboratories, Fort Eustis, VA, 1966.

[20] Raymer, D. P., *Aircraft Design: A Conceptual Approach, 5th Edition*, AIAA, 2012.

[21] FAA, "14 CFR 91.151 - Fuel requirements for flight in VFR conditions." https://www.law.cornell.edu/cfr/text/14/91.151, 2017.

[22] Gudmundsson, S., *General Aviation Aircraft Design: Applied Methods and Procedures*, Butterworth-Heinemann, 2013.

[23] "Aurora Flight Sciences Showcases New eVTOL Aircraft," http://www.auvsi.org/blogs/auvsi-news/2017/04/25/aurora-flight-sciences-showcases-new-evtol-aircraft, 2017.

[24] "Carter partners with Mooney for Uber Elevate air taxi concept," https://www.verticalmag.com/press-releases/carter-partners-mooney-uber-elevate-air-taxi-concept/, 2017.

[25] "Airbus has a secret flying-car project called Vahana," https://www.theverge.com/2016/10/21/13357690/airbus-flying-car-vahana-a-cubed-autonomous-taxi, 2016.

[26] "Joby S2," http://www.jobyaviation.com/S2/, 2016.

[27] "R44 Raven Series," http://www.robinsonheli.com/rhc_r44_raven_series.html, 2016.

[28] "Kamov Ka32," https://barrieaircraft.com/kamov-ka32.html, 2017.

[29] Bennett, J., "EHang Wants You to Fly in Their Autonomous Drone," http://www.popularmechanics.com/flight/drones/a18865/ehang-184-fly-in-autonomous-drone/, 2017.

[30] "M-16 Tandem Trainer," http://www.magnigyro.com/models/m16.html, 2017.

[31] "Lilium Aviation," https://lifeboat.com/blog/2016/05/lilium-aviation, 2016.

[32] Duffy, M. J., Wakayama, S. R., Hupp, R., Lacy, R., and Stauffer, M., "A Study in Reducing the Cost of Vertical Flight with Electric Propulsion," Conference Paper, 17th AIAA Aviation Technology, Integration, and Operations Conference, Denver, CO, 2017.

[33] "BLADE - The Sharpest Way to Fly," https://www.flyblade.com/, 2017.

[34] "New York City Helicopter Tours," https://www.newyorkhelicopter.com/, 2017.

[35] "SkyVector: Flight Planning / Aeronautical Charts," https://skyvector.com/, 2017.

[36] Vascik, P. D. and Hansman, R. J., "Evaluation of Key Operational Constraints Affecting On-Demand Mobility for Aviation in the Los Angeles Basin: Ground Infrastructure, Air Traffic Control and Noise," Conference Paper, 17th AIAA Aviation Technology, Integration, and Operations Conference, AIAA AVIATION Forum, Denver, CO, 2017.

[37] Campbell, M., "Patent filings detail Retina MacBook Pro's quiet asymmetric fans," http://appleinsider.com/articles/12/12/20/patent-filings-detail-retina-macbook-pros-quiet-asymmetric-fans, 2012.

[38] Moore, M. D. and Fredericks, B., "Misconceptions of Electric Propulsion Aircraft and Their Emergent Aviation Markets," Conference Paper, AIAA SciTech, 2014.

[39] FAA, "U.S. Civil Airmen Statistics," https://www.faa.gov/data_research/aviation_data_statistics/civil_airmen_statistics/, 2016.

[40] Herniczek, M. K., Feszty, D., Meslioui, S.-A., and Park, J., "Applicability of Early Acoustic Theory for Modern Propeller Design," Conference Paper, 23rd AIAA/CEAS Aeroacoustics Conference, AIAA AVIATION Forum, Denver, CO, 2017.

[41] "Prediction Procedure for Near-Field and Far-Field Propeller Noise," Technical Standard AIR1407, Society of Automotive Engineers, 1977.